Adaptive optics ophthalmoscopy: application to age-related macular degeneration and vascular diseases

Michel Paques, Serge Meimon, Florence Rossant, David Rosenbaum, Sarah Mrejen, Florian Sennlaub, Kate Grieve

Adaptive optics ophthalmoscopy: application to age-related macular degeneration and vascular diseases

Michel Paques[1], Serge Meimon[2], Florence Rossant[3], David Rosenbaum[4], Sarah Mrejen[1], Florian Sennlaub[5], Kate Grieve[1]

[1]Centre Hospitalier National d'Ophtalmologie des Quinze-Vingts, INSERM-DHOS Clinical Investigation Center 1423, Paris, France.

[2]ONERA - The French Aerospace Lab, 92320 Châtillon, France

[3]Institut Supérieur d'Electronique de Paris, 75006 Paris, France

[4]Unité de prévention cardiovasculaire, Salpêtrière Hospital, UPMC Univ Paris 06

[5]Institut de la Vision, 17 rue Moreau, Sorbonne Universités, UPMC Univ Paris 06, INSERM, CNRS, 75012 Paris, France.

†Correspondence should be addressed to: Prof Michel Paques, Paris Adaptive Optics Retinal Imaging and Surgery (PARIS) group; Tel: (33) 1 40 02 14 15 Fax: (33) 1 53 46 26 93; Email: mp@cicoph.org

Adaptive optics ophthalmoscopy: application to age-related macular degeneration and vascular diseases

Abstract

Adaptive optics (AO)-enhanced *en face* retinal imaging, termed here AO ophthalmoscopy (AOO) has reached a level of robustness which fosters its expanding use in research and clinical centers. Here we will review the contribution of clinical AOO to the understanding and monitoring of 1) age-related macular degeneration and 2) vascular diseases. The main contributions of AOO to the phenotyping of AMD are a better identification of drusen, a better delineation of the limits of atrophy, and the identification of novel features such as punctate hyperreflectivity and mobile melanin clumps. Characterization of progression of atrophy is facilitated by time-lapse AOO. In vessels AOO imaging enables the observation and measurement of parietal structures and the observation of microscopic pathological features such as small hemorrhages and inflammatory cell accumulations.

Contents

1. Introduction

The first observation of the fundus of the eye in the nineteenth century led to the foundation of modern ophthalmology. Until recently, however, the retina itself could not be directly observed because it is translucent and hence faintly visible by fundus photography. It was the advent of techniques allowing a higher contrast such as optical coherence tomography (OCT) in the 1990s and then adaptive optics (AO)-enhanced ophthalmoscopy (AOO) in the 2000s that made neuroretinal structures directly observable in vivo. The first demonstration of the clinical interest of AOO was reported in 1997 in Liang, Miller and William's seminal work using an AO fundus camera[1] which allowed observation of cone photoreceptors. Since then, by achieving diffraction-limited resolution in clinically usable, robust systems, visualization of previously unseen structures such as individual photoreceptors and vessel walls can now be done in a routine fashion. Thanks to the convergence of technical maturity and better understanding of the contribution of AOO imaging, its use in research and clinical centers is expanding worldwide, in ophthalmology and beyond. Several reviews of AOO have been done previously[2-5]. In the present review, we will focus on the contribution of AOO to the understanding of age-related macular degeneration (AMD) and vascular diseases, and suggest some perspectives for improvement in these areas. We will limit this review to en face fundus camera and scanning AOO systems, excluding adaptive optics optical coherence tomography (AO-OCT) which has not yet been applied to the same extent to AMD and vasculature in patients. Readers interested in AO-OCT may refer to several reviews[6,7].

2. AO ophthalmoscopy (AOO) technologies

High resolution imaging of the retina faces several challenges, including optical aberrations arising from the anterior segment and the limited reflectance of the retina. These challenges are tackled by AO which counteracts optical aberrations in real-time with a

deformable mirror, whose shape is derived from wavefront measurements via a real-time control loop, in order to increase light throughput and resolution. AOO has been performed with flood illumination fundus cameras, scanning laser ophthalmoscopes (SLO) and OCT[6,7]. Fundus camera systems use flood illumination to capture a two dimensional en face image in a single shot using a two dimensional camera as detector. SLO systems scan point by point (or line by line) in a raster fashion over the retina and collect the backscattered light with a single-pixel detector. Fundus camera and scanning AOO systems yield different results (**Fig. 1**). Fundus camera images show inherently less motion-induced distortion than scanning systems, which is of interest in the case of poor fixation, at the cost of reduced contrast. The main advantage of SLO systems is the use confocal detection to reject light from out of focus layers and so achieve high axial resolution and contrast. SLO systems have also benefitted from alternative detection schemes (known as split detection, offset aperture or dark field) that capture multiply scattered photons that do not pass through the confocal pinhole. Eliminating the strongest signal, which tends to emanate from directionally dependent waveguided light from photoreceptor outer segments and the highly scattering nerve fibers and vessels, enables detection of more weakly reflective structures, for example photoreceptor inner segments[8], retinal pigment epithelium (RPE)[9,10] and retinal ganglion cells[11].

In the text that follows, for scanning AOO images we will call the directly backscattered light that passes through the confocal pinhole the "bright field" mode, and the multiply scattered light which is offset from the confocal pinhole the "dark field" mode. The ability to separate the different sources of contrast in these different modalities can provide clues as to the origin of the features we observe and hence their clinical signification.

3. Dry age-related macular degeneration

AMD is a leading cause of blindness in developed countries[12,13]. Despite the identification of several genetic, molecular and environmental factors[14,15], the pathophysiology of AMD

remains debated and in its dry form there is currently no available treatment. Histopathological changes of dry AMD affect the outer retina, the RPE and the inner choroid[16]. The dominant paradigm states that AMD results from cumulative damage affecting the interaction between the photoreceptors and the RPE cells related to genetically determined low grade subretinal inflammation[17]. Over decades, cumulative low level damage challenges the resilience of the outer retina; the sight-threatening complications of AMD are therefore the clinical manifestation of a rupture and/or exhaustion of chronically activated compensatory mechanisms.

Clinically, an early/intermediate phase moderately affecting vision is followed by a late stage at which sight-threatening complications are observed. Funduscopically, the canonical lesions of early/intermediate AMD are drusen and/or pseudodrusen, basal linear deposits (which are focal thickening of the Bruch's membrane) and pigmentary changes. Transition from early to late dry AMD occurs when spots of Bruch's membrane devoid of RPE are detected. The disruption of the RPE monolayer (grographic atrophy) is indeed the key event leading to blindness, because it is temporally and spatially linked to loss of cones and to the advent of an absolute scotoma[18]. Here, we will describe the most notable contributions of AOO to the phenotyping of AMD, and compare the knowledge about histology and pathophysiology of dry AMD to AOO. Most of the histology data presented here is from the Project Macula developed by Christine Curcio and the University of Alabama of Birmingham (www. *projectmacula.cis.uab.edu*)[19].

3.1. Early stage AMD

Drusen are composed of focal deposits of extracellular debris in contact with the RPE. Drusen are hallmarks of AMD. Each druse subtype bears a specific risk of evolution to late stages of AMD. Three main drusen phenotypes have been characterized: either under the RPE ("conventional" soft drusen, and cuticular drusen) or over the RPE (subretinal drusenoid

deposits (SDD, also called reticular pseudodrusen). Spaide, Curcio and co-authors have hypothesized that their different imaging and histologic characteristics are due to differences in location and biogenesis[20-23].

Figure 2 illustrates the fundus camera AOO appearance of the different types of drusen by comparison with non-AO corrected near infrared (nIR) SLO images. Conventional drusen appear on AOO as subtle variations in the grayscale tones, with a variably hyperreflective center. Drusen are usually surrounded by a continuous or discontinuous hyporeflectivity and sometimes an incomplete dark ring. Some conventional drusen appeared more reflective than others, with a better contrast from the background areas[24,25]. Cone photoreceptors are detected overlying conventional drusen and the cone density has been found to be moderately reduced over conventional drusen. The differences in reflectivity of conventional drusen may be due to differences in sub-RPE material reflectivity as these variations can be seen on SD-OCT as well, and also to variable degrees of depigmentation and thinning of the overlying RPE. These hypotheses need to be further investigated through mutlimodal imaging integrating nIR autofluorescence to evaluate the degrees of RPE degeneration associated with conventional drusen. Some authors showed that RPE atrophy predates the collapse of large conventional drusen by analysing the sequence of events in OCT over time.[26,27]

Cuticular drusen correspond to the innumerable mosaic of small and uniformly sized drusen visualized on fluorescein angiography (FA) and indocyanine green (ICG) angiography. With AOO their reflectivity profile is variable; they may appear as a hyporeflective center with a hyperreflective rim or diffusely hyperreflective. Different patterns of reflectivity could be found in the same eye, as has also been described with nIR scanning laser ophthalmoscopy (SLO)[28]. These different reflectivity aspects found within the same eye could correspond either to different evolutive stages or to different types of cuticular drusen, but also to the degree of depigmentation and thinning of the overlying RPE.

SDD have a specific reflectivity in AOO, with a hyperreflective core of variable size circled by a dark rim of constant width; this aspect has been confirmed on both fundus camera and scanning AOO systems. In addition, numerous dark dots can be visualized around the areas of larger SDD that were not visualized around conventional drusen with AOO or other imaging modalities; these may correspond to smaller stage 1 or 2 SDD not discriminated with conventional nIR SLO imaging. Meadway et al analyzed the microstructure of stage 3 SDD using scanning AOO and AO OCT and showed that the speckled appearance over SDD of grossly similar shape and reflectivity as photoreceptors was rather due to the granules of the lesion material itself[29]. AOO helped demonstrate that SDD were composed of material that accumulates in the same tissue compartment as photoreceptors above the RPE and associated with major perturbations of photoreceptors. Zhang et al also demonstrated the dynamism of SDD with scanning AOO over 12 months, analyzing 269 solitary SDD in 6 eyes of 4 patients[30]. They showed that there were new and regressed SDD lesions over time and that the percentage of sampled retinal areas affected by these ranged from 0.7% to 9.3%.

A peculiar situation is small drusen of young subjects. On bright field scanning AOO images, these drusen appear as round, oval or lobular areas of diameter 22-61 µm where cone photoreceptor reflectivity and density are decreased[31] usually associated with discrete thickening of the RPE complex. The outline and size of these lesions corresponds to 1-4 RPE cells, hence giving rise to the hypothesis that small, hard drusen could arise from very few RPE cells. When high in density, these may represent the earliest stage of druse; yet the extent to which these findings apply to age-related drusen remains to be determined.

3.2 Late AMD ("geographic atrophy")

3.2.1 Atrophy margins

Figure 3 shows an example of montage of fundus camera AOO images of a dry AMD case. **Figure 4** compares the different modalities of AOO imaging. The margins of atrophic

areas show a variety of aspects, ranging from well-defined to ill-defined (**Figure 5**). With fundus camera AOO, well-defined margins are often hyporeflective, further enhancing their contrast and also suggesting that they contain melanin clumps; it is however possible that retinal disorganization also contributes to the hyporeflectivity of the margins. Ill-defined atrophy margins on the other hand are very difficult to delineate unambiguously. In these cases, tracing a limit between the preserved RPE monolayer and the atrophic area is highly subjective, particularly if there are overlapping foci of hyporeflective clumps (HRCs). These HRCs are indeed more numerous in ill-defined than in well-defined borders. During the follow-up of AMD patients, comparing successive AOO images can demonstrate progression of atrophic lesions within a relatively short time frame (**Fig. 6**)[32].

The persistence of an "island' of intact RPE monolayer under the fovea in the midst of an area of RPE atrophy, called foveal sparing, is often observed. Despite the preservation of central visual acuity, the resulting tunnel-like vision is often a severe handicap. Conceivably, in these cases even a small progression of RPE atrophy towards the fovea will be associated with severe visual loss. While short wavelength autofluorescence imaging is impaired by the presence of the xanthophyll pigment which blurs the limits of preserved RPE[33,34], AOO enables an exquisite delineation of such areas[32,35] (**Fig. 4**).

3.2.2 Cone mosaic and punctate hyperreflectivity

In preserved areas of dry AMD eyes, the cone mosaic is often dim in AOO images, with a high spatial variability of reflectivity; such poor visibility of the cone mosaic is further accentuated at the edge of GA lesions[36]. It remains uncertain if the altered visibility is due to the actual loss of cones or to the alteration of their optical properties. Histology shows that cones at lesion margins have altered morphology[16,37, 38] which may contribute to their poor visibility. This poor visibility of the cone mosaic is in striking contrast with the observation of a bright hyperreflective granular structure within atrophic regions mimicking the normal cone

194 photoreceptor mosaic. This is consistently observed on different cases, with both fundus
195 camera and scanning AOO (**Fig. 7**) although the bright field mode of scanning AOO yields
196 the highest contrast for this specific feature. The density of such punctate hyperreflectivity
197 (PHR) is within the range of the normal cone density (unpublished data). Since PHR
198 resembles the cone mosaic, it may correspond to photoreceptor remnants. Histology studies of
199 AMD indeed showed that in atrophic areas there may be remnants of cone inner segments[39].
200 However, these inner segments remnants are sparse, irregularly dispersed and lack outer
201 segments which make them unlikely to have such a bright hyperreflectance and regular
202 disposition.

203 Basal laminar deposits (BlamD) are sub-RPE deposits that are a hallmark of the aging
204 Bruch's membrane[40]. They are made of a continuous material deposition between the RPE
205 basal membrane and Bruch's membrane. When devoid of RPE cells, the BlamD may persist
206 and form a continuous layer which is spiky on its inner surface and smooth on its outer
207 surface[41, 42] (i.e. in contact with Bruch's membrane) (**Fig. 8**). Hence, reflectance over the
208 BlamD may theoretically generate a mosaic-like reflectance similar to the PHR. In order to
209 better understand the origin of PHR, directional imaging may be helpful since the Stiles-
210 Crawford effect may facilitate the identification of cone photoreceptors[43,44]. If the BlamD is
211 indeed involved, then the similarity of the PHR and cone mosaic raises the question of the
212 possible interference of the reflectance from both structures (i.e., the cone mosaic and BlamD)
213 in non-atrophic areas. This may contribute to the abovementioned poor visibility of the cone
214 mosaic.

215 3.2.3. Hyporeflective clumps (HRCs)

216 Fundoscopic examination and histology shows that extensive melanin redistribution
217 accompanies all stages of AMD[37,45]. In histology this is seen in the earliest steps of AMD in
218 the form of rearrangement of intracellular melanosomes, leading to an uneven distribution of

melanin. During late AMD, more marked changes can be observed, the most remarkable being the presence of hyporeflective clumps (HRCs) dispersed over the RPE monolayer as well as within atrophic areas. These HRCs have been attributed to detached RPE cells[37] and/or to a non-RPE cell type (possibly microglia[46,47] or monocyte-macrophages that have phagocytized RPE cells[48]). Many HRCs indeed show cytological characteristics very close to those of RPE cells; at the same time, the unequivocal presence of subretinal and sub-RPE macrophages identified using immunohistological markers such as CD163, IBA-1 and CCR2[48,49] have been reported in eyes with dry AMD. A significant number of subretinal macrophages indeed contain melanosomes, presumably from ingested RPE cells. It is possible that HRCs in the outer nuclear layer account for the hyperflective foci seen with OCT during AMD[46]. A histological taxonomy of human HRCs based on their shape and location has been recently proposed[19]. This classification distinguishes bilaminar, sloughed, dissociated, shedding, and entombed types.

A consistent feature of AO fundus camera images of dry AMD is the presence of a myriad of HRCs dispersed over the posterior pole (**Fig. 5 and 9**). Although the size of HRCs varies greatly, they typically appear as black dots measuring around 20µm[32] , hence similar to the size of melanin containing cells seen in histology. As histology suggests that melanosomes remain mostly intracellular even at late stages of the disease, HRCs can be considered as intracellular tags for most of them. HRCs can be detected over the atrophic areas as well as over the RPE monolayer (albeit with a lower contrast in the latter case). It is surprising to note that HRCs are of low contrast in scanning AOO; HRCs are indeed much better detected by fundus camera AOO than by scanning AOO (**Fig. 9**).

HRCs appear to colocalize with hyper-nIR autofluorescence (nIRAF)[32,50], although the colocalization of HRCs and hyper-nIRAF can at present only be hypothesized based on comparison of images of unequal resolution. Use of an nIRAF-capable AOO system such as

that used in (Granger, Williams, Rossi, ARVO E-abstract 3429, 2017) could provide an answer to this question.

When comparing successive AOO fundus images of dry AMD taken over a period of several months, extensive changes in the distribution of HRCs are consistently observed. When adequate time sampling is done (i.e. at a rate of approximately one image per month), time-lapse sequences unequivocally demonstrate that there is motion of many HRCs[32]. Migration of HRCs is the most dynamic process that has been identified to date in AMD; it can indeed be detected over a timescale of days while atrophy progression is only detectable over a timescale of weeks. One may hypothesize that such activity represents a reactive process following degeneration. In this regard, it is of interest to note that migration of HRCs is also observed over non atrophic areas (i.e. over the intact RPE monolayer). This indicates that such cell motility may be present early in the course of AMD, and hence is not solely an effect of cone photoreceptor degeneration. The velocity of HRCs is highly heterogeneous, and can reach a magnitude of one micrometer a day. They show a complex migration that defies classification. Most show limited, erratic motion, while some seem to progress in parallel to atrophy progression. Very few show a directional progression (**Fig. 10 and 11**). The significance of such motion is uncertain; displacement of HRCs may not necessarily imply that an entire cell is moving. Indeed, intracellular motion of melanosomes may account for <10μm scale motion of HRCs. To our knowledge there is very limited documentation of cell migration in the living retina. It has been showed that microglial and infiltrating macrophage cells can migrate in response to damage to the RPE[47].

Although it is a speculative approach, some correspondence between this taxonomy and AOO imaging of HRCs may be postulated (**Fig. 12**). Along progression fronts, cells in the pigmented borders are probably of the “bilaminar” phenotype, i.e. with a layer of HRCs over the RPE monolayer. Highly contrasted HRCs dispersed over the RPE monolayer outside of

margins are possibly HRCs of the "sloughed" type. Similar HRCs over RPE atrophy may be cells of the "dissociated" type. The migration pattern of HRCs may also contribute to classify them into this taxonomy. Migration is probably facilitated in the subretinal space; it may therefore be assumed that HRCs of the "sloughed" phenotype are more likely to show migration. On the other hand, "subducted" HRCs (i.e. located between the BlamD and the Bruch's membrane) are probably less mobile because they are embedded in remodeled tissues. Very small static melanin spots may be "shed RPE cells", i.e. whose melanosomes are embedded into subretinal material.

3.2.4 Outer retinal tubulations

Within atrophic areas there are frequently tubular, 50-100µm wide arborescent structures , termed outer retinal tubulations (ORT)[51]. ORTs contain radially oriented cones and Müller cell extensions[52-54]. The presence of ORTs shows that cones may survive for a relatively long duration in atrophic areas. Fundus camera and scanning AOO can both detect the outlines of ORTs (**figure 13**)[55]. It has been shown that scanning AOO can detect cone structure within ORTs[56]. It has been postulated that this configuration is a survival strategy for cones[49] albeit their potential for functional recovery is unknown. The possibility of detecting (and hence monitoring) surviving cones within ORTs may be of interest to characterize the resilience of cones in dystrophic retinas, and may also guide RPE grafting since an area with cone persistence may be most appropriate.

3.3 Perspectives for AOO of dry AMD

The complex features of dry AMD are progressively being unveiled using a variety of imaging techniques, among which AOO will probably play a major role. Investigating the correspondence of AOO images with histology will be crucial to improve the rationale for their interpretation.

293 Current cell culture technology can achieve a functionally and phenotypically normal RPE
294 mosaic[57], and even sub-RPE deposits mimicking drusen[58]. Hence, it can be expected that
295 imaging RPE cell cultures may be an acceptable surrogate for *in vivo* imaging of RPE aging
296 and diseases.
297 A higher short-wavelength autofluorescence signal along lesional margins is predictive of
298 progression[59]. En face imaging of tissue samples offers some useful support for image
299 interpretation, showing for instance the colocalization of lipofuscin and melanin at a
300 microscopic level (**Figure 14**).[60,61] One can hence speculate that accumulation of HRCs along
301 the margins of atrophy may be linked to the increased short wavelength autofluorescence.
302 Hence, the link between short-wavelength autofluorescence and AMD progression is possibly
303 explained by the presence of HRCs at the margins of atrophy. Accordingly, a recent clinical
304 study suggested that pigmentary changes are predictive of progression.[62]
305 Analyzing the migration of HRCs is still a challenge. It is known that HRCs may migrate
306 into the inner retina[19] and hence escape the focus plane of AOO. Therefore, migrating patterns
307 of HRCs may be more accurately defined by taking into consideration their depth disposition
308 within the retinal layers as well. Time-lapse volumetric OCT may therefore contribute to a
309 better tracking of HRCs within the depth of the retina, while AOO may be most suitable for
310 those migrating close to the RPE.
311 In vivo observation of the RPE cells is still far from being a routine procedure, although it
312 has recently shown interesting perspectives using AO-enhanced indocyanine green
313 angiography[63], AO-enhanced short wavelength[10] and infrared autofluorescence[64] and two-
314 photon imaging[65]. Given that technical robustness and absence of light toxicity is
315 demonstrated, this may be of interest to analyze the fate of individual RPE cells, which would
316 help to clarify the origin of HRCs. The choriocapillaris is still difficult to analyze in detail in
317 vivo although AO-OCT[66] has recently shown interesting perspectives. Finally, wet AMD is

still difficult to explore with AOO because of the combination of loss of retinal transparency and the complex 3D arrangement of lesions.

4. Vascular imaging

The retina relies on a finely tuned blood flow for its supply of metabolites and metabolic signals and for disposal of waste products. The planar disposition of retinal vessels make them conveniently observable with *en face* imaging. The exponential relationship between lumen diameter and conductance (Poiseuille's law) highlights the importance of high precision measurement of vascular diameters. The retinal vessels are cognates of brain vessels, sharing many functional and pathological features; hence, retinal vessels may be considered in many aspects as surrogates of brain vessels. Age, hypertension and diabetes are the most common factors influencing the morphology and function of microvessels. With the advent of AOO, not only did measurement of lumen diameter with micrometric precision become possible, but also structural imaging[67]. Dedicated software for automated segmentation of arteries has been developed which facilitates the extraction of clinically relevant biomarkers.[68]

4. 1 Normal vessels

AOO imaging of vessels shows the red blood cell column as a dark line with a specular reflex along its crest. Along arteries and sometimes along veins, the walls can be seen as thin, laminated bands (**Fig. 15**). With fundus camera AOO, there is also a hyperreflective halo surrounding the vessels, possibly due to the backscattering of laterally reflected incident light. It is thought that the inner limit of the wall corresponds to the plasma-endothelial interface, and that the outer limit represents the outer limit of the adventicia. Within the wall of arteries a central hyporeflective band can be identified (**Fig. 16**) which possibly corresponds to the media containing smooth muscle cells[67]. This central hyporeflective band is more apparent over lightly pigmented RPE (not shown), highlighting the role of backscattered light in its

visualization. AOO can also detect discrete structures (**Fig. 16, right**), presumably comprising pericytes.

AOO offered for the first time the possibility to measure directly the thickness of the wall and hence to calculate the wall-to-lumen ratio (WLR) in vivo[69]. Assuming a correct anatomical correspondence, the median WLR of normal arterioles is ~0.28; WLR increases when the size of the artery decreases[70]. The WLR of normal veins is around 0.1; no lamination has been yet observed in the venous wall.

At arterial bifurcations, the specular reflex along the vessel crest is divided along daughter branches, while at venous confluences each specular reflex can be followed after the confluence (**Fig**. **17**).[71] This demonstrates that red blood cells, which remain in distinct columns after venous confluences, contribute to the axial specular reflex.

The geometry of the arteriolar arborescence is an essential determinant of its energetic efficiency[72]. Based on the minimal work principle, Murray's laws state that for achieving the conflictual requirements of minimization of shear stress and blood volume, blood flow should be proportional to the cube of the vessel radii[73]. Because of the conservation of flow, this implies that at arterial bifurcations there is a cubic relationship between the radii of parent (P) and daughter vessels (D_1 and D_2). Hence in a symmetrical bifurcation there is a homothetical factor (i.e. a relative variation of diameter of downstream vessels) of 0.79. These laws, established on theoretical grounds, were verified in vivo only in the 1970s[74]. The junction coefficient (X solving $P^x=D_1^x + D_2^x$, for which the expected value is 3) is a convenient way of quantifying the conformation of a microvascular network to Murray's laws. **Figure 18** illustrates the changes in X consecutive to changes in vessel diameters in an optimal bifurcation. This shows that an increased X means a better conductance of flow downward to the bifurcation, either because of an increased daughter (D) or a decreased parent (P). Hence, at a particular bifurcation, deviation of X from 3 parallels flow conductance.

In retinal vessels, deviation from optimality has been associated with peripheral arterial diseases[75], incident heart disease, stroke[76] and diabetes[77], yet these conclusions were drawn from conventional fundus photographs; hence blur may have altered the precision of the measurements. Using AOO, in normal arteries a median value of X of 2.8 in arteries and of 2.3 in veins has been reported[78], both being significantly inferior to 3. The cause of this physiological deviation from Murray's laws remains to be determined.

Retinal capillaries have a complex, multilayered 3D arrangement. A serial arrangement of these layers has been documented in rodents[79,80] and pigs[81], yet remains to be confirmed in the primate retina. Fine details of capillaries are visible with bright field scanning AOO but are only faintly detectable with AOO fundus cameras[82]. Offset imaging with motion contrast has proven effective to image capillaries.[83,84] Indeed, differential analysis between two images specifically detects fast moving particles, that is, red blood cells. Viewing of retinal capillaries using oral fluorescein angiography has also been demonstrated[85]. **Figure 19** shows an example of a montage of scanning AOO images of capillaries. AOO is not yet capable of imaging wide field volumes to cover the whole complex 3D retinal capillary network. Nevertheless, capillary imaging and flow measurements in the perifoveal ring have a clear clinical interest because of the disproportional importance of the fovea for vision relative to its size. The flow of leukocytes in individual capillaries and the flow in the perifeoveal capillaries has been reported[86,87] in which velocities between 0 and 1.2mm/sec were measured. By using a combination of scanning AOO and computational fluid dynamics analysis, it has been shown that wall shear stress can be estimated in vivo in human perifoveal capillaries[88].

4. 2 Vascular aging and hypertension

The most common manifestations of aging/hypertensive retinopathy are diffusely increased WLR and focal lesions such as focal arteriolar narrowings (FANs) and

arteriovenous nickings (AVNs). These features have been the subject of a considerable amount of research as predictive biomarkers of end-organ damage[89]. Several large scale epidemiological studies reported that the severity and/or incidence of these signs correlate with end-organ damage[90]. Hypertensive microvasculopathy is also suspected to play a role in Alzheimer's disease[91]. It is of importance to note that atherosclerosis (atheroma), i.e. the presence in the subintima of cholesterol plaques, affects only large arteries and hence does not affect retinal vessels.

4.2.1 Parietal thickening

The WLR of arterioles is a fundamental indicator of the effect of arterial hypertension on small vessels. Increased WLR occurs through the chronic stimulation by blood pressure of the myogenic reflex (Bayliss effect)[92], a process leading to eutrophic remodelling. Fundus photograph-based studies reported an age and pressure-related decline of the lumen diameter of arteries, which may be interpreted as indirect evidence of parietal thickening[93]. However, despite some interesting results using differential Doppler and reflectance imaging[92], until the advent of AOO, there was no convenient clinical method to measure the WLR. Since then, several teams have shown that the WLR measured with AOO correlates well with blood pressure[69,95-98]. Ageing also decreases the diameter of the lumen and the parietal thickness, hence increasing the WLR. The effect of blood pressure on the WLR is therefore age-dependant, with a stronger correlation in young subjects[95].

Measurement of the WLR in the retina appears to be an interesting tool for management of arterial hypertension. Since change in the WLR occurs in a matter of weeks, it is rather immune to acute changes in blood pressure; hence, it is possible that the WLR is an integrator of past blood pressure. Considering the WLR may thus help to overcome the problem of stress-induced variation of blood pressure (so-called "white coat hypertension"). After a few weeks of antihypertensive treatment introduction, a significant increase in internal diameter

was reported[95] leading to a decreased WLR. Interestingly, this was observed irrespective of the pharmacological class, suggesting that the effect of antihypertensive drugs on small vessels is mediated by blood pressure, rather than through a direct pharmacological effect on small vessels. AOO has been used to detect short-term changes in vascular morphometry following surgical treatment of resistant hypertension[99].

4.2.2 Focal vascular lesions: arteriovenous nickings and focal arteriolar narrowing

While most scientific research and hence conceptual efforts in hypertensive microvasculopathy are addressed to diffuse changes of parietal thickness, little attention is paid to focal microvascular changes. This is partly due to the fact that these changes are difficult to capture with histology. Moreover, their natural history is poorly documented.

Narrowing and deformation of veins in the vicinity of arteries defines AVNs. The latter are surrogates of cerebrovascular aging and are also the direct cause of retinal vein occlusions. There has been a longstanding yet unsubstantiated consensus among clinicians about the compressive nature of the arteriovenous conflict underlying AVNs. This belief persists despite the fact that histology studies failed to evidence arteriovenous compression; instead, histology consistently pointed to extravascular changes identified as glial proliferation, glial edema[100] or extracellular deposits[101], as the cause of AVNs.

Using AOO we have shown that the WLR does not differ between AVNs and normal arteriovenous crossings, ruling out parietal thickening as the cause of AVNs[69]. However, to analyze the interface between an artery and a vein at an arteriovenous crossing, optical access to the interface is necessary, which is usually not possible using reflectance imaging because the interposition of the artery. This can be overcome by analyzing a specific yet uncommon vascular pattern, that is, cases in which focal venous remodeling is observed where an artery and a vein are close yet not overlapping ; these cases can reasonably be considered as "non-

crossing" AVNs[102]. Indeed, veins adjacent to arterioles may undergo marked phenotypical changes identical to AVNs (i.e. nicking, narrowing, opacification and/or dragging) without any physical arteriovenous contact as demonstrated by AOO (**Fig. 20**). These findings support and extend the conclusions of histology stating that the paradigm of arterial crushing as the cause of venous nicking stems from a misinterpretation of fundus photographs.

During aging, irregularities in the caliber of arteries are also commonly observed. The most obvious manifestation is the presence of FANs, i.e. a clinically detectable focal reduction of arteriolar caliber. Given the exponential relationship between lumen diameter and flow conductance, even a limited, focal reduction in diameter may have significant hemodynamic consequences. Theoretically, FANs may be due to parietal thickening or focal vasoconstriction. In all cases of FANs that we examined, the outer limit of the wall remained parallel to the internal wall (**Fig. 20, top)**, that is, there was no evidence of local parietal thickening. Moreover, we frequently observed disappearance of FANs (**Fig. 20, bottom**), which strongly argues for chronic vasoconstriction being the cause of FANs. The presence of FANs may thus be an indicator of a dysregulation of the microvascular tone.

4. 3 Diabetic retinopathy

Diabetic retinopathy (DR) is a leading cause of visual loss in working-age adults worldwide[103-105]. Histology shows that loss of pericytes and endothelial cells occur early in DR, being detectable in experimental diabetes long before there is any macroscopic sign of DR. DR is hence considered as resulting from the cumulative effect of progressive loss of canonical functions of retinal capillaries leading to a combination of nonperfusion and hyperpermeability. The very first clinically detectable changes seen in vivo are microaneurysms surrounded by capillary occlusions.

AOO is promising for the detection of early capillary changes. At the earliest stages of DR (i.e. in the absence of clinically gradable diabetic retinopathy), capillary dilation[106],

tortuosity[83, 107] and disruption of capillaries[108] have been reported. A higher flow velocity than controls has also been reported.[109] Recently, alteration of the junction coefficient has been confirmed by an AOO study in diabetics[78].

The internal structure of microaneurysms has been explored with scanning AOO using a combination of reflectance and fluorescence angiography[107]. This study showed that microaneurysms have a variably thickened wall. At more advanced stages of DR, an exquisitely fine documentation of microscopic features such as microaneurysms, microhemorrages, and hard exudates (**Fig.21**) can also be obtained with AOO.

4. 4 Vascular inflammation

Because vessels are physiologically in contact with innate and adaptive immune effectors, they are at the crossroads of a variety of inflammatory diseases. Accordingly, retinal vascular inflammation is a common feature during various types of uveitis, which can be detected on fundus images under the form of perivascular sheathing and/or focal disruption of the blood-retinal barrier. Veins are more often affected than arteries by inflammation. Post-capillary venules are the elective site of extravasation of blood-borne inflammatory cells (diapedesis). Given the diagnostic and prognostic value of perivascular sheathing, it would be of clinical interest to better identify, quantify and monitor retinal vasculitis. Thanks to the high sensitivity of AO to loss of retinal transparency, paravascular cellular infiltrates constitutive of retinal vasculitis can be detected with high precision (**Fig. 22**).[110] Perivascular inflammation can be located on one or both sides of vessels, over a width of several tens of micrometers, up to several millimeters along the affected vessel. Focal reduction of venous diameter often accompanies perivascular sheathing. In the example showed in **figure 23**, perivascular sheathing was accompanied by local deformation of the adjacent NFL, suggesting that in this particular case venous narrowing may have been due to compression from the infiltrate.

4. 5 Perspectives for AOO in vascular imaging

Because microvascular structure, motricity and flow can be analyzed with AOO with high precision, a better knowledge of the pathophysiology of human microvasculature will undoubtedly emerge from future clinical studies and technological development based on AOO. Fine morphometric measurements are a promising approach because they may enable identification of subtle changes of perfusion homeostasis at an early stage.

The complex spatial and functional organization of retinal capillaries makes comprehensive mapping of retinal microvessels challenging with AAO; on the other hand, a better understanding of this organization will enable the design of specific procedures. For instance, the deep vascular layer is electively affected by capillary remodelling in DR[111] and retinal vein occlusions[80,112]. Postcapillary venules, which are located for the most part in this same layer are also the preferential site of leukocyte adherence and diapedesis. Hence, targeting the deep microvessel layer may offer more precise insights into several processes affecting microvessels. Similarly, targeting the perifoveal capillaries may be relevant for diseases affecting the macula.

The oxygen saturation of red cells can be measured in the retina using differential light absorption[113]. Current techniques for oxymetry, however, are limited to medium to large vessels; in the future, AOO-enhanced oxymetry techniques may provide access to oxygen saturation of capillaries. Measuring the biomechanics of the systolic pulse on retinal vessels offers an interesting approach for evaluating the stiffness of large vessels. It is possible to document microvasculature caliber and tortuosity changes during the cardiac cycle with scanning AOO[67] and fundus camera AOO[114]. Such mechanotransmission has been the subject of extensive studies in the cardiovascular field[115] since it is believed that the velocity of the systolic pulse is related to parietal stiffness.

The natural history of early stages microvascular aging, of DR and of hypertensive retinopathy remains poorly documented with AOO. At the earliest stages of DR, AOO study of capillary flow may help to solve controversies about retinal blood flow changes[116,117]. Functional studies at the capillary level (neurovascular coupling[118]) may also be of interest, as a decreased efficiency of neurovascular coupling in the retina is present early in diabetes[119]. Longitudinal AOO studies may contribute to a better knowledge of the natural history of the development of microaneurysms, capillary nonperfusion and exudates. In particular, documenting the loss of pericytes[71] offers also interesting perspectives.

5. AOO in clinical trials

Clinical trials in ophthalmology increasingly rely on imaging. More precise biomarkers allow earlier results with fewer patients, and are therefore ethically necessary. However, while the use of OCT in clinical trials has been developing at an exponential pace, AO-enhanced imaging has lagged behind. The current technological level of robustness and the possibility to obtain quantitative biomarkers already permits the integration of AO in large scale trials in AMD, arterial hypertension and vasculitis. For trials in AMD, emergence and progression of small atrophic spots are the most straightforward applications. A particular interest of AOO is to enable precise monitoring of the residual RPE in cases of foveal sparing. Cell therapy using RPE cell grafts has been proposed to treat atrophic AMD[120]; time-lapse AOO would be of interest to follow the fate of grafted cells. In arterial hypertension, WLR is a robust, dimensionless parameter that can be measured on large cohorts of nondilated patients. Several epidemiological studies on retinal vessel imaging using AO, including pediatric cohorts, are underway. A promising perspective of AOO is the follow-up of patients treated by antihypertensive drugs. The retina indeed offers the unique possibility to measure the effect of vasoactive drugs. It would be of interest to determine if early ‘microvascular responders’ (i.e., those patients showing vasodilation under therapy) have a better prognosis in terms of

reduction of end-organ damage. In inflammatory diseases, the size of inflammatory infiltrates around vessels may also be considered as a biomarker of interest. The contribution of AOO to trials in diabetic retinopathy is promising. For instance, AOO may better document the turnover of microaneurysms; another application would be the measurement of the morphometry of arterial bifurcations.

6. Conclusions

Most medical specialists can only dream of the highly precise imaging that we ophthalmologists can routinely achieve using AOO. AOO may force us to rethink the physiopathological concepts of many diseases affecting the retina. As Sydney Brenner said, "progress in science depends on new techniques, new discoveries and new ideas, probably in that order". By enabling quantitative in vivo "optical biopsy", high resolution imaging may find many medical applications in a spectrum of indications, spanning from ophthalmology to general medicine. The possibility to perform a fine quantitative analysis is of obvious interest for monitoring diseases. Diseases that show slow progression at a macroscopic scale can reveal significantly more activity at a smaller scale. The applications of AOO to other public health diseases such as arterial hypertension and diabetes will bring support from the pharmaceutical industry which may further boost clinical developments of AOO.

AOO is a rapidly changing field and the range of its medical applications is constantly increasing[1]; the reader should therefore keep in mind that our review is at risk of rapid obsolescence. For instance, while long considered unfeasible, visualization of human retinal ganglion cells[11] was recently demonstrated. There are still several hurdles that hinder the full integration of AOO in routine clinics and trials. Several factors such as technical complexity, cost, interpretative schemes and integration of AOO images into management of patients still need to be improved. These topics are the subject of a multidisciplinary effort of physicists, computer scientists, ophthalmologists, and histologists. Improving knowledge of histology

and of light-tissue interactions will be useful. Investigation of light-tissue interactions using similar techniques in vitro and in vivo[121] will help to improve the rationale of image interpretation. Among other questions is the fact that structures may have a different aspect in scanning and fundus camera AOO. Acquiring more clinical experience, using accurate metrics and building large normative databases will improve image interpretation. Image processing and analysis software should be customized to diseases and biomarkers and combine multimodal information. Then, more adequate training schemes, standard procedures, and biomarkers for trials may be developed. Trials in healthcare domains other than ophthalmology will be facilitated with the use of user-friendly, automated, nonmydriatic instruments.

Acknowledgements

Jonathan Benesty, Celine Chaumette, Marie-Hélène Errera, Elena Gofas-Salas, Céline Faure, Xavier Girerd, Edouard Koch, Chahira Miloudi, Pedro Mecê, Hasan Sawan, José-Alain Sahel, Valérie Sarda, Andrea Sodi, Iyed Trimèche and the patients that participated in our studies.

This work was supported by the Institut National de la Santé et de la Recherche Médicale (Contrat d'Interface 2011), the Agence Nationale de la Recherche (ANR-12-TECS-0015-03, LabEx LIFESENSES ANR-10-LABX-65, ANR-11-IDEX-0004-02), the Foundation Fighting Blindess (C-CL-0912-0600-INSERM01, C-GE-0912-0601-INSERM02), the Thome Foundation and the European Research Council (ERC-SyG 610110). The funding organization had no role in the design or conduct of this research. Original data provided here are from a clinical research study (ClinicalTrials.gov NCT0154618).

References

1. Liang, J., Williams, D. R. & Miller, D. T. Supernormal vision and high-resolution retinal imaging through adaptive optics. *J. Opt. Soc. Am. A Opt. Image Sci. Vis.* **14,** 2884–2892 (1997).

2. Roorda A. Applications of adaptive optics scanning laser ophthalmoscopy. Optom Vis Sci. 2010 Apr; 87(4):260-8.

3. Godara P, Dubis AM, Roorda A, Duncan JL, Carroll J. Adaptive Optics Retinal Imaging: Emerging Clinical Applications. Optom Vis Sci. 2010;87(12):930-941.

4. Roorda, A. & Duncan, J. L. Adaptive optics ophthalmoscopy. *Annu. Rev. Vis. Sci.* **1,** 19–50 (2015)

5. Marcos, S. *et al.* Vision science and adaptive optics, the state of the field. *Vision Res.* **132,** 3–33 (2017).

6. Jonnal R. S. *et al.* A Review of Adaptive Optics Optical Coherence Tomography: Technical Advances, Scientific Applications, and the Future. *Invest. Ophthalmol. Vis. Sci.* **57,** 51-68

7. Pircher M, Zawadzki RJ. Review of adaptive optics OCT (AO-OCT): principles and applications for retinal imaging [Invited]. Biomed Opt Express. 2017 Apr 19;8(5):2536-2562

8. Scoles, D. *et al.* In vivo imaging of human cone photoreceptor inner segments. *Invest. Ophthalmol. Vis. Sci.* **55,** 4244–4251 (2014).

9. Scoles, D., Sulai, Y. N. & Dubra, A. In vivo dark-field imaging of the retinal pigment epithelium cell mosaic. *Biomed. Opt. Express* **4,** 1710–1723 (2013).

10. Rossi, E. A. *et al.* In vivo imaging of retinal pigment epithelium cells in age related macular degeneration. *Biomed. Opt. Express* **4,** 2527–2539 (2013).

11. Rossi, E. A. *et al.* Imaging individual neurons in the retinal ganglion cell layer of the living eye. *Proc. Natl. Acad. Sci. U. S. A.* **114,** 586–591 (2017).

12. Robman, L. D. *et al.* Age-related macular degeneration in ethnically diverse Australia: Melbourne Collaborative Cohort Study. *Ophthalmic Epidemiol.* **22,** 75–84 (2015).

13. Klein, R. *et al.* Prevalence of age-related macular degeneration in the US population. *Arch. Ophthalmol. Chic. Ill 1960* **129,** 75–80 (2011).

14. Ardeljan, D. & Chan, C.-C. Aging is not a disease: distinguishing age-related macular degeneration from aging. *Prog. Retin. Eye Res.* **37,** 68–89 (2013).

15. Ambati, J. & Fowler, B. J. Mechanisms of age-related macular degeneration. *Neuron* **75,** 26–39 (2012)

16. Bird, A. C., Phillips, R. L. & Hageman, G. S. Geographic atrophy: a histopathological assessment. *JAMA Ophthalmol.* 132, 338–345 (2014).

17. Guillonneau X, Eandi CM, Paques M, Sahel JA, Sapieha P, Sennlaub F. On phagocytes and macular degeneration. Prog Ret Eye Res 2017;61: 98-128.

18. Panorgias, A. *et al.* Multimodal assessment of microscopic morphology and retinal function in patients with geographic atrophy. *Invest. Ophthalmol. Vis. Sci.* **54,** 4372–4384 (2013).

19. Zanzottera, E. C. *et al.* The Project MACULA Retinal Pigment Epithelium Grading System for Histology and Optical Coherence Tomography in Age-Related Macular Degeneration. *Invest. Ophthalmol. Vis. Sci.* **56,** 3253–3268 (2015).

20. Spaide RF, Curcio CA. Drusen characterization with multimodal imaging. Retina. 2010;30:1441-1454.

21. Curcio CA, Messinger JD, Sloan KR, et al. Subretinal drusenoid deposits in non-neovascular age-related macular degeneration: morphology, prevalence, topography, and biogenesis model. Retina. 2013;33:265-276

22. Spaide RF, Curcio CA, Zweifel SA. Drusen, an old but new frontier. Retina. 2010;30:1163-1165.

638 23. Zweifel SA, Spaide RF, Curcio CA, et al. Reticular pseudodrusen are subretinal
639 drusenoid deposits. Ophthalmology. 2010;117:303-312 e301
640 24. Mrejen, S., Sato, T., Curcio, C. A. & Spaide, R. F. Assessing the cone photoreceptor
641 mosaic in eyes with pseudodrusen and soft Drusen in vivo using adaptive optics
642 imaging. *Ophthalmology* **121,** 545–551 (2014).
643 25. Querques, G. *et al.* Appearance of medium-large drusen and reticular pseudodrusen on
644 adaptive optics in age-related macular degeneration. *Br. J. Ophthalmol.* **98,** 1522–1527
645 (2014).
646 26. Balaratnasingam C, Messinger JD, Sloan KR, et al. Histologic and Optical Coherence
647 Tomographic Correlates in Drusenoid Pigment Epithelium Detachment in Age-Related
648 Macular Degeneration. Ophthalmology. 2017;124:644-656.
649 27. Balaratnasingam C, Yannuzzi LA, Curcio CA, et al. Associations Between Retinal
650 Pigment Epithelium and Drusen Volume Changes During the Lifecycle of Large
651 Drusenoid Pigment Epithelial Detachments. Invest Ophthalmol Vis Sci. 2016;57:5479-
652 5489
653 28. Balaratnasingam C, Cherepanoff S, Dolz-Marco R, et al. Cuticular Drusen: Clinical
654 Phenotypes and Natural History Defined Using Multimodal Imaging. Ophthalmology.
655 2018;125:100-118.
656 29. Meadway, A., Wang, X., Curcio, C. A. & Zhang, Y. Microstructure of subretinal
657 drusenoid deposits revealed by adaptive optics imaging. *Biomed. Opt. Express* **5,** 713–
658 727 (2014)
659 30. Zhang, Y. *et al.* DYNAMISM OF DOT SUBRETINAL DRUSENOID DEPOSITS IN
660 AGE-RELATED MACULAR DEGENERATION DEMONSTRATED WITH
661 ADAPTIVE OPTICS IMAGING. *Retina Phila. Pa* **38,** 29–38 (2018)

31. Pedersen, H. R. *et al.* Multimodal imaging of small hard retinal drusen in young healthy adults. *Br. J. Ophthalmol.* **102,** 146–152 (2018).

32. Gocho, K. *et al.* Adaptive optics imaging of geographic atrophy. *Invest. Ophthalmol. Vis. Sci.* **54,** 3673–3680 (2013).

33. Schmitz-Valckenberg, S. *et al.* In vivo imaging of foveal sparing in geographic atrophy secondary to age-related macular degeneration. *Invest. Ophthalmol. Vis. Sci.* **50,** 3915–3921 (2009).

34. Lindner, M. *et al.* Directional Kinetics of Geographic Atrophy Progression in Age-Related Macular Degeneration with Foveal Sparing. *Ophthalmology* **122,** 1356–1365 (2015).

35. Querques, G. *et al.* ADAPTIVE OPTICS IMAGING OF FOVEAL SPARING IN GEOGRAPHIC ATROPHY SECONDARY TO AGE-RELATED MACULAR DEGENERATION. *Retina Phila. Pa* **36,** 247–254 (2016). ^

36. Zayit-Soudry, S., Duncan, J. L., Syed, R., Menghini, M. & Roorda, A. J. Cone structure imaged with adaptive optics scanning laser ophthalmoscopy in eyes with nonneovascular age-related macular degeneration. *Invest. Ophthalmol. Vis. Sci.* **54,** 7498–7509 (2013)

37. Zanzottera, E. C. *et al.* VISUALIZING RETINAL PIGMENT EPITHELIUM PHENOTYPES IN THE TRANSITION TO GEOGRAPHIC ATROPHY IN AGE-RELATED MACULAR DEGENERATION. *Retina Phila. Pa* **36 Suppl 1,** S12–S25 (2016).

38. Eandi CM, Messance HC, Augustin S, Dominguez E, Lavalette S, Forster V, Hu SJ, Siquieros L, Craft CM, Sahel JA, Tadayoni R, Paques M, Guillonneau X, Sennlaub F. Subretinal mononuclear phagocytes induce cone segment loss via IL-1β. eLife 2016;5:e16490

39. Curcio, C. A., Medeiros, N. E. & Millican, C. L. Photoreceptor loss in age-relatedmacular degeneration. *Invest. Ophthalmol. Vis. Sci.* **37,** 1236–1249 (1996).

687 40. Sarks, S., Cherepanoff, S., Killingsworth, M. & Sarks, J. Relationship of Basal Laminar
688 Deposit and Membranous Debris to the Clinical Presentation of Early Age-Related
689 Macular Degeneration. *Invest. Ophthalmol. Vis. Sci.* **48,** 968–977 (2007).
690 41. Tan ACS, Astroz P, Dansingani KK, Slakter JS, Yannuzzi LA, Curcio CA, Bailey
691 Freund K. The Evolution of the Plateau, an Optical Coherence Tomography Signature
692 Seen in Geographic Atrophy. *Invest. Ophthalmol. Vis. Sci.* 2017;58:2349-2358.
693 42. Ooto S, Vongkulsiri S, Sato T, Suzuki M, Curcio CA, Spaide RF. Outer Retinal
694 Corrugations in Age-Related Macular Degeneration. JAMA Ophthalmol.
695 2014;132(7):806-813.
696 43. Panorgias, A. *et al.* Multimodal assessment of microscopic morphology and retinal
697 function in patients with geographic atrophy. *Invest. Ophthalmol. Vis. Sci.* **54,** 4372–4384
698 (2013).
699 44. Miloudi, C. *et al.* The Negative Cone Mosaic: A New Manifestation of the Optical
700 Stiles-Crawford Effect in Normal Eyes. *Invest. Ophthalmol. Vis. Sci.* **56,** 7043–7050
701 (2015).
702 45. Zanzottera, E. C., Messinger, J. D., Ach, T., Smith, R. T. & Curcio, C. A. Subducted and
703 melanotic cells in advanced age-related macular degeneration are derived from retinal
704 pigment epithelium. *Invest. Ophthalmol. Vis. Sci.* **56,** 3269–3278 (2015).
705 46. Curcio, C. A., Zanzottera, E. C., Ach, T., Balaratnasingam, C. & Freund, K. B.
706 Activated Retinal Pigment Epithelium, an Optical Coherence Tomography Biomarker
707 for Progression in Age-Related Macular Degeneration. *Invest. Ophthalmol. Vis. Sci.* **58,**
708 BIO211-BIO226 (2017).
709 47. Paques, M. *et al.* In vivo observation of the locomotion of microglial cells in the retina.
710 *Glia* **58,** 1663–1668 (2010).

48. Sennlaub, F. *et al.* CCR2(+) monocytes infiltrate atrophic lesions in age-related macular disease and mediate photoreceptor degeneration in experimental subretinal inflammation in Cx3cr1 deficient mice. *EMBO Mol. Med.* **5,** 1775–1793 (2013).

49. Combadière, C. *et al.* CX3CR1-dependent subretinal microglia cell accumulation is associated with cardinal features of age-related macular degeneration. *J. Clin. Invest.* **117,** 2920–2928 (2007).

50. Kellner, U., Kellner, S. & Weinitz, S. Fundus autofluorescence (488 NM) and near-infrared autofluorescence (787 NM) visualize different retinal pigment epithelium alterations in patients with age-related macular degeneration. *Retina Phila. Pa* **30,** 6–15 (2010).

51. Zweifel, S. A. *et al.* Outer retinal tubulation: a novel optical coherence tomography finding. *Arch. Ophthalmol. Chic. Ill 1960* **127,** 1596–1602 (2009).

52. Litts, K. M. *et al.* Clinicopathological correlation of outer retinal tubulation in age-related macular degeneration. *JAMA Ophthalmol.* **133,** 609–612 (2015).

53. Litts, K. M., Messinger, J. D., Freund, K. B., Zhang, Y. & Curcio, C. A. Inner Segment Remodeling and Mitochondrial Translocation in Cone Photoreceptors in Age-Related Macular Degeneration With Outer Retinal Tubulation. *Invest. Ophthalmol. Vis. Sci.* **56,** 2243–2253 (2015).

54. Litts, K. M. *et al.* Quantitative Analysis of Outer Retinal Tubulation in Age-Related Macular Degeneration From Spectral-Domain Optical Coherence Tomography and Histology. *Invest. Ophthalmol. Vis. Sci.* **57,** 2647–2656 (2016).

55. Litts, K. M. *et al.* EXPLORING PHOTORECEPTOR REFLECTIVITY THROUGH MULTIMODAL IMAGING OF OUTER RETINAL TUBULATION IN ADVANCED AGE-RELATED MACULAR DEGENERATION. *Retina Phila. Pa* **37,** 978–988 (2017).

56. King, B. J. *et al.* SD-OCT and Adaptive Optics Imaging of Outer Retinal Tubulation. *Optom. Vis. Sci. Off. Publ. Am. Acad. Optom.* **94,** 411–422 (2017).

736 57. Reichman, S. *et al.* Generation of Storable Retinal Organoids and Retinal Pigmented
737 Epithelium from Adherent Human iPS Cells in Xeno-Free and Feeder-Free Conditions. *Stem*
738 *Cells Dayt. Ohio* **35,** 1176–1188 (2017).
739 58. Pilgrim, M. G. *et al.* Subretinal Pigment Epithelial Deposition of Drusen Components
740 Including Hydroxyapatite in a Primary Cell Culture Model. *Invest. Ophthalmol. Vis. Sci.* **58,**
741 708–719 (2017)
742 59. Holz, F. G. *et al.* Progression of geographic atrophy and impact of fundus
743 autofluorescence patterns in age-related macular degeneration. *Am. J. Ophthalmol.* **143,** 463–
744 472 (2007).
745 60. Pollreisz, A. *et al.* Visualizing melanosomes, lipofuscin, and melanolipofuscin in human
746 retinal pigment epithelium using serial block face scanning electron microscopy. *Exp. Eye*
747 *Res.* **166,** 131–139 (2017).
748 61. Holz, F. G., Steinberg, J. S., Göbel, A., Fleckenstein, M. & Schmitz-Valckenberg, S.
749 Fundus autofluorescence imaging in dry AMD: 2014 Jules Gonin lecture of the Retina
750 Research Foundation. *Graefes Arch. Clin. Exp. Ophthalmol. Albrecht Von Graefes Arch. Klin.*
751 *Exp. Ophthalmol.* **253,** 7–16 (2015).
752 62. Ferrara, D. *et al.* Optical Coherence Tomography Features Preceding the Onset of
753 Advanced Age-Related Macular Degeneration. *Invest. Ophthalmol. Vis. Sci.* **58,** 3519–3529
754 (2017).
755 63. Tam, J., Liu, J., Dubra, A. & Fariss, R. In Vivo Imaging of the Human Retinal Pigment
756 Epithelial Mosaic Using Adaptive Optics Enhanced Indocyanine Green Ophthalmoscopy.
757 *Invest. Ophthalmol. Vis. Sci.* **57,** 4376–4384 (2016).
758 64. Morgan, J. I. W., Dubra, A., Wolfe, R., Merigan, W. H. & Williams, D. R. In Vivo
759 Autofluorescence Imaging of the Human and Macaque Retinal Pigment Epithelial Cell
760 Mosaic. *Invest. Ophthalmol. Vis. Sci.* **50,** 1350–1359 (2009).

761 65. Sharma, R., Williams, D. R., Palczewska, G., Palczewski, K. & Hunter, J. J. Two-
762 Photon Autofluorescence Imaging Reveals Cellular Structures Throughout the Retina of the
763 Living Primate Eye. *Invest. Ophthalmol. Vis. Sci.* **57,** 632–646 (2016).
764 66. Kurokawa, K., Liu, Z. & Miller, D. T. Adaptive optics optical coherence tomography
765 angiography for morphometric analysis of choriocapillaris [Invited]. *Biomed. Opt. Express* **8,**
766 1803 (2017).
767 67. Chui, T. Y. P., Gast, T. J. & Burns, S. A. Imaging of vascular wall fine structure in the
768 human retina using adaptive optics scanning laser ophthalmoscopy. *Invest. Ophthalmol. Vis.*
769 *Sci.* **54,** 7115–7124 (2013).
770 68. Lermé, N. *et al.* A fully automatic method for segmenting retinal artery walls in adaptive
771 optics images. *Pattern Recognit. Lett.* **72,** 72–81 (2016).
772 69. Koch, E. *et al.* Morphometric analysis of small arteries in the human retina using
773 adaptive optics imaging: relationship with blood pressure and focal vascular changes. *J.*
774 *Hypertens.* **32,** 890–898 (2014).
775 70. Meixner, E. & Michelson, G. Measurement of retinal wall-to-lumen ratio by adaptive
776 optics retinal camera: a clinical research. *Graefes Arch. Clin. Exp. Ophthalmol. Albrecht Von*
777 *Graefes Arch. Klin. Exp. Ophthalmol.* **253,** 1985–1995 (2015).
778 71. Chui, T. Y. P., Vannasdale, D. A. & Burns, S. A. The use of forward scatter to improve
779 retinal vascular imaging with an adaptive optics scanning laser ophthalmoscope. *Biomed. Opt.*
780 *Express* **3,** 2537–2549 (2012).
781 72. Murray, C. D. The Physiological Principle of Minimum Work: I. The Vascular System
782 and the Cost of Blood Volume. *Proc. Natl. Acad. Sci. U. S. A.* **12,** 207–214 (1926).
783 73. Mayrovitz, H. N. & Roy, J. Microvascular blood flow: evidence indicating a cubic
784 dependence on arteriolar diameter. *Am. J. Physiol.* **245,** H1031-1038 (1983).

74. Zamir, M., Medeiros, J. A. & Cunningham, T. K. Arterial bifurcations in the human retina. *J. Gen. Physiol.* **74,** 537–548 (1979).

75. Chapman, N. *et al.* Peripheral vascular disease is associated with abnormal arteriolar diameter relationships at bifurcations in the human retina. *Clin. Sci. Lond. Engl. 1979* **103,** 111–116 (2002).

76. Witt, N. W. *et al.* A novel measure to characterise optimality of diameter relationships at retinal vascular bifurcations. *Artery Res.* **4,** 75–80 (2010).

77. Sasongko, M. B. *et al.* Alterations in retinal microvascular geometry in young type 1 diabetes. *Diabetes Care* **33,** 1331–1336 (2010).

78. Luo, T., Gast, T. J., Vermeer, T. J. & Burns, S. A. Retinal Vascular Branching in Healthy and Diabetic Subjects. *Invest. Ophthalmol. Vis. Sci.* **58,** 2685–2694 (2017).

79. Paques, M. *et al.* Structural and hemodynamic analysis of the mouse retinal microcirculation. *Invest. Ophthalmol. Vis. Sci.* **44,** 4960–4967 (2003).

80. Genevois, O. *et al.* Microvascular remodeling after occlusion-recanalization of a branch retinal vein in rats. *Invest. Ophthalmol. Vis. Sci.* **45,** 594–600 (2004).

81. Fouquet, S., Vacca, O., Sennlaub, F. & Paques, M. The 3D Retinal Capillary Circulation in Pigs Reveals a Predominant Serial Organization. *Invest. Ophthalmol. Vis. Sci.* **58,** 5754–5763 (2017).

82. Lombardo, M. *et al.* Analysis of retinal capillaries in patients with type 1 diabetes and nonproliferative diabetic retinopathy using adaptive optics imaging. *Retina Phila. Pa* **33,** 1630–1639 (2013).

83. Tam, J., Martin, J. A. & Roorda, A. Noninvasive visualization and analysis of parafoveal capillaries in humans. *Invest. Ophthalmol. Vis. Sci.* **51,** 1691–1698 (2010).

808 84. Sulai, Y. N., Scoles, D., Harvey, Z. & Dubra, A. Visualization of retinal vascular
809 structure and perfusion with a nonconfocal adaptive optics scanning light ophthalmoscope. *J.*
810 *Opt. Soc. Am. A Opt. Image Sci. Vis.* **31,** 569–579 (2014).
811 85. Pinhas, A. *et al.* In vivo imaging of human retinal microvasculature using adaptive
812 optics scanning light ophthalmoscope fluorescein angiography. *Biomed. Opt. Express* **4,**
813 1305–1317 (2013).
814 86. Martin, J. A. & Roorda, A. Direct and noninvasive assessment of parafoveal capillary
815 leukocyte velocity. *Ophthalmology* **112,** 2219–2224 (2005).
816 87. Arichika, S., Uji, A., Ooto, S., Miyamoto, K. & Yoshimura, N. Adaptive optics-assisted
817 identification of preferential erythrocyte aggregate pathways in the human retinal
818 microvasculature. *PloS One* **9,** e89679 (2014).
819 88. Lu, Y. *et al.* Computational fluid dynamics assisted characterization of parafoveal
820 hemodynamics in normal and diabetic eyes using adaptive optics scanning laser
821 ophthalmoscopy. *Biomed. Opt. Express* **7,** 4958–4973 (2016).
822 89. Hanff, T. C. *et al.* Retinal microvascular abnormalities predict progression of brain
823 microvascular disease: an atherosclerosis risk in communities magnetic resonance imaging
824 study. *Stroke* **45,** 1012–1017 (2014).
825 90. Yatsuya, H. *et al.* Retinal microvascular abnormalities and risk of lacunar stroke:
826 Atherosclerosis Risk in Communities Study. *Stroke* **41,** 1349–1355 (2010).
827 91. Cheung, C. Y.-L., Ong, Y.-T., Ikram, M. K., Chen, C. & Wong, T. Y. Retinal
828 microvasculature in Alzheimer's disease. *J. Alzheimers Dis. JAD* **42 Suppl 4,** S339-352
829 (2014).
830 92. Heagerty, A. M., Aalkjaer, C., Bund, S. J., Korsgaard, N. & Mulvany, M. J. Small artery
831 structure in hypertension. Dual processes of remodeling and growth. *Hypertens. Dallas Tex*
832 *1979* **21,** 391–397 (1993).

833 93. Kawasaki, R. *et al.* Retinal vessel diameters and risk of hypertension: the Multiethnic
834 Study of Atherosclerosis. *J. Hypertens.* **27,** 2386–2393 (2009).
835 94. Harazny, J. M. *et al.* New software analyses increase the reliability of measurements of
836 retinal arterioles morphology by scanning laser Doppler flowmetry in humans. *J. Hypertens.*
837 **29,** 777–782 (2011).
838 95. Rosenbaum, D. *et al.* Effects of age, blood pressure and antihypertensive treatments on
839 retinal arterioles remodeling assessed by adaptive optics. *J. Hypertens.* **34,** 1115–1122 (2016).
840 96. Rosenbaum, D. *et al.* Relationships between retinal arteriole anatomy and aortic
841 geometry and function and peripheral resistance in hypertensives. *Hypertens. Res. Off. J. Jpn.*
842 *Soc. Hypertens.* **39,** 536–542 (2016).
843 97. Hillard, J. G., Gast, T. J., Chui, T. Y. P., Sapir, D. & Burns, S. A. Retinal Arterioles in
844 Hypo-, Normo-, and Hypertensive Subjects Measured Using Adaptive Optics. *Transl. Vis.*
845 *Sci. Technol.* **5,** (2016).
846 98. Arichika, S., Uji, A., Ooto, S., Muraoka, Y. & Yoshimura, N. Effects of age and blood
847 pressure on the retinal arterial wall, analyzed using adaptive optics scanning laser
848 ophthalmoscopy. *Sci. Rep.* **5,** 12283 (2015).
849 99. Gallo, A., Rosenbaum, D., Kanagasabapathy, C. & Girerd, X. Effects of carotid
850 baroreceptor stimulation on retinal arteriole remodeling evaluated with adaptive optics camera
851 in resistant hypertensive patients. *Ann. Cardiol. Angeiol. (Paris)* **66,** 165–170 (2017).
852 100. Kimura, T., Mizota, A., Fujimoto, N. & Tsuyama, Y. Light and electron microscopic
853 studies on human retinal blood vessels of patients with sclerosis and hypertension. *Int.*
854 *Ophthalmol.* **26,** 151–158 (2005).
855 101. Jefferies, P., Clemett, R. & Day, T. An anatomical study of retinal arteriovenous
856 crossings and their role in the pathogenesis of retinal branch vein occlusions. *Aust. N. Z. J.*
857 *Ophthalmol.* **21,** 213–217 (1993).

858 102. Paques, M. *et al.* Venous Nicking Without Arteriovenous Contact: The Role of the
859 Arteriolar Microenvironment in Arteriovenous Nickings. *JAMA Ophthalmol.* **133,** 947–950
860 (2015).
861 103. Raman, R., Gella, L., Srinivasan, S. & Sharma, T. Diabetic retinopathy: An epidemic at
862 home and around the world. *Indian J. Ophthalmol.* **64,** 69–75 (2016).
863 104. Grauslund, J., Green, A. & Sjølie, A. K. Blindness in a 25-year follow-up of a
864 population-based cohort of Danish type 1 diabetic patients. *Ophthalmology* **116,** 2170–2174
865 (2009).
866 105. Cheung, N., Mitchell, P. & Wong, T. Y. Diabetic retinopathy. *Lancet Lond. Engl.* **376,**
867 124–136 (2010).
868 106. Burns, S. A. *et al.* In vivo adaptive optics microvascular imaging in diabetic patients
869 without clinically severe diabetic retinopathy. *Biomed. Opt. Express* **5,** 961–974 (2014)
870 107. Dubow, M. *et al.* Classification of human retinal microaneurysms using adaptive optics
871 scanning light ophthalmoscope fluorescein angiography. *Invest. Ophthalmol. Vis. Sci.* **55,**
872 1299–1309 (2014).
873 108. Tam, J. *et al.* Disruption of the retinal parafoveal capillary network in type 2 diabetes
874 before the onset of diabetic retinopathy. *Invest. Ophthalmol. Vis. Sci.* **52,** 9257–9266
875 (2011).
876 109. Arichika, S. *et al.* Retinal hemorheologic characterization of early-stage diabetic
877 retinopathy using adaptive optics scanning laser ophthalmoscopy. *Invest. Ophthalmol. Vis.*
878 *Sci.* **55,** 8513–8522 (2014).
879 110. Errera, M.-H. *et al.* Retinal vasculitis imaging by adaptive optics. *Ophthalmology* **121,**
880 1311–1312.e2 (2014).

111. Couturier, A. *et al.* CAPILLARY PLEXUS ANOMALIES IN DIABETIC RETINOPATHY ON OPTICAL COHERENCE TOMOGRAPHY ANGIOGRAPHY. *Retina Phila. Pa* **35,** 2384–2391 (2015).

112. Suzuki, N. *et al.* Microvascular Abnormalities on Optical Coherence Tomography Angiography in Macular Edema Associated With Branch Retinal Vein Occlusion. *Am. J. Ophthalmol.* **161,** 126–132.e1 (2016).

113. Linsenmeier, R. A. & Zhang, H. F. Retinal oxygen: from animals to humans. *Prog. Retin. Eye Res.* **58,** 115–151 (2017).

114. Duan, A., Bedggood, P. A., Metha, A. B. & Bui, B. V. Reactivity in the human retinal microvasculature measured during acute gas breathing provocations. *Sci. Rep.* **7,** (2017).

115. Vlachopoulos, C. *et al.* The role of vascular biomarkers for primary and secondary prevention. A position paper from the European Society of Cardiology Working Group on peripheral circulation: Endorsed by the Association for Research into Arterial Structure and Physiology (ARTERY) Society. *Atherosclerosis* **241,** 507–532 (2015).

116. Burgansky-Eliash, Z. *et al.* Reduced retinal blood flow velocity in diabetic retinopathy. *Retina Phila. Pa* **30,** 765–773 (2010).

117. Burgansky-Eliash, Z. *et al.* Increased retinal blood flow velocity in patients with early diabetes mellitus. *Retina Phila. Pa* **32,** 112–119 (2012).

118. Newman, E. A. Functional hyperemia and mechanisms of neurovascular coupling in the retinal vasculature. *J. Cereb. Blood Flow Metab. Off. J. Int. Soc. Cereb. Blood Flow Metab.* **33,** 1685–1695 (2013).

119. Lecleire-Collet, A. *et al.* Evaluation of retinal function and flicker light-induced retinal vascular response in normotensive patients with diabetes without retinopathy. *Invest. Ophthalmol. Vis. Sci.* **52,** 2861–2867 (2011).

120. Schwartz, S. D., Tan, G., Hosseini, H. & Nagiel, A. Subretinal Transplantation of Embryonic Stem Cell-Derived Retinal Pigment Epithelium for the Treatment of Macular Degeneration: An Assessment at 4 Years. *Invest. Ophthalmol. Vis. Sci.* **57,** ORSFc1-9 (2016).

121. Grieve, K., Thouvenin, O., Sengupta, A., Borderie, V. M. & Paques, M. Appearance of the Retina With Full-Field Optical Coherence Tomography. *Invest. Ophthalmol. Vis. Sci.* **57,** OCT96-OCT104 (2016).

Figure legends

Figure 1: Comparison of fundus camera (left column) vs bright field scan (right column) AOO, showing normal photoreceptors (top row), an artery (center row), and an atrophy zone during dry age-related macular degeneration.

Figure 2. Imaging of drusen. Top row, near infrared scanning laser ophthalmoscopy (nIR SLO) imaging; center row, OCT; bottom row, fundus camera AOO. (A, D, G) Conventional drusen appear as subtle variations in the grayscale tones surrounded by discontinuous hyporeflectivity on the fundus camera AOO. (B, E, H) cuticular drusen distributed in a continuous pattern are clearly distinguished on corresponding AOO. (C, F, I) subretinal drusenoid deposits (SDD) are visible by AOO as hyperreflective cores of variable sizes surrounded by dark annulus of constant width. Some of the dark dots (arrows) may correspond to smaller stage 1 or 2 SDD.

Figure 3: Montage of fundus camera AOO images of a case of dry AMD.

Figure 4. Case of foveal sparing seen by SLO, OCT, fundus camera AOO and scanning AOO in bright and dark field modes.

Figure 5. Example of ill-defined (top) and well-defined (bottom) lesions viewed with fundus camera AOO.

Figure 6: Illustration of progression of GA. (A) SLO infrared image. (B, C) two AOO fundus camera images taken 1 month apart. The horizontal lines and the arrow in (C) facilitate the identification of the progression of atrophy. Note also the rearrangement of HRCs outside of the atrophic area (compare the pattern of pigment distribution in the circles) (from [32]).

Figure 7: Top: AOO fundus camera imaging of a GA case illustrating the similarities between punctuate hyperreflectivity (PHR) and the cone mosaic (CM). The dotted line represents the progression front. Note that some HRCs are superimposed with the PHR. Bottom, comparison of flood versus bright field scan AOO of the PHR and presumed CM at

941 the border of an atrophic lesion. While the CM is dim in bright field scan and/or blurred in
942 fundus camera AOO, within the atrophy areas there is a hyperreflective granular structure (i.e.
943 the PHR) of appearance and spacing similar to the CM.
944 **Figure 8**. Histology of BlamD (arrowheads) in an atrophic area of a GA eye (from
945 *projectmacula.cis.uab.edu).* Note the spiky surface of the BlamD.
946 **Figure 9**: Comparison of fundus camera versus scanning AOO of HRCs. Fundus camera
947 AOO shows HRCs as dark spots, while with scanning AOO they are less contrasted (arrows).
948 **Figure 10:** Example of migration patterns of HRCs (arrows) seen by fundus camera AOO.
949 Top row: migration in parallel to the progression of atrophy (b, c, and d: zoom of the area
950 shown in a, showing the progression of atrophy over 6 months). Bottom row: linear
951 progression (g: recapitulation over 8 months).
952 **Figure 11**: Illustration of the migration of an HRC (solid arrowhead) ahead of atrophy
953 progression seen by fundus camera AOO. The hollow arrowhead recapitulates the successive
954 position of the HRC s in previous images.
955 **Figure 12**: Comparison of histology and AOO images of a case of dry AMD. Presumptive
956 RPE cell types described by Zanzoterra et al.[19] are shown.
957 **Figure 13**: Outer retinal tubulations (ORT) seen with fundus camera AOO (A) and by bright
958 and dark field scanning AAO (B and C respectively). A: ORT in a case of dry AMD
959 (delineated by arrowheads). B and C, ORT in a case of retinal dystrophy. A long ORT (black
960 arrows) and several smaller ORT (white arrows) are seen extending from the less abnormal
961 region of retina into the atrophic region. Inserted are magnifications of the bright and dark
962 field, respectively, showing cones extending onto the ORT (Scale bars = 200 μm) (modified
963 from [56])

Figure 14. Illustration of the colocalization of short-wavelength autofluorescence (lipofuscin) and melanin in a retinal flat-mount of a GA case. The upper row shows immunolabelling of the actin cytoskeleton indicating confluence of RPE cells (modified from [37]).

Figure 15. AOO fundus camera imaging of a normal arteriovenous pair. In the magnifications, arrowheads show the arterial and venous wall.

Figure 16: Details of parietal structures in an arteriole obtained by fundus camera AOO (left; from author Serge Meimon) and with an offset aperture AOSLO (modified from [67]). Note details of fine parietal structures, which may correspond to mural cells (black arrows).

Figure 17: Imaging of venous confluences showing the alignment of red blood cell columns. Left, fundus camera AOO image. Three red blood cell columns (numerated 1 to 3) can be followed in pre and post-confluence vessels. Center and right, scanning AOO bright and dark motion contrast image (TBC), respectively. In the latter note the presence of at least three distinct red cell columns (from[71]).

Figure 18: Mathematical relationship between the variations of vessel diameter on the junction coefficient at an optimal bifurcation with initial values for the parent vessel (P) of 100µm and for daughter vessels (D_1 and D_2) of 79.37µm (which implies X=3). Each curve represents the variations of X following the variation of the diameter of one vessel (P or D_1). Overall, an increased X implies an increased downstream conductance which may be due to upstream constriction or downstream dilation. For instance when P increases by 10µm, X will increase to ~ 4.

Figure 19. Montage scanning AOO bright field image of the perifoveal capillaries using motion contrast (from [108]) (scale bar, 250µm).

Figure 20: Fundus camera AOO images of venous nicking with (left) and without (center) arteriovenous overlapping. Note in the central image the absence of detectable arteriovenous

contact. Right, focal arterial narrowing (FAN); zoom shows that the inner and outer limits of the wall remain parallel within the FAN.

Figure 21: Examples of fundus camera AAO imaging of advanced diabetic retinopathy showing from left to right microaneurysms, hard exudates and microhemorrhages.

Figure 22: Fundus camera AOO montage showing paravenous infiltrates (arrows) in a case of idiopathic vasculitis.

Figure 23: Evolution of a paravenous inflammatory infiltrate. A: fluorescein angiography; B: Fundus camera AOO showing in the boxed area a perivenous infiltrate. C to D: follow-up on the perivenous infiltrate. Note that the resolution of the infiltrate seems to coincide with restauration of venous caliber and also with the resolution of the displacement of axonal fibers (arrowheads).

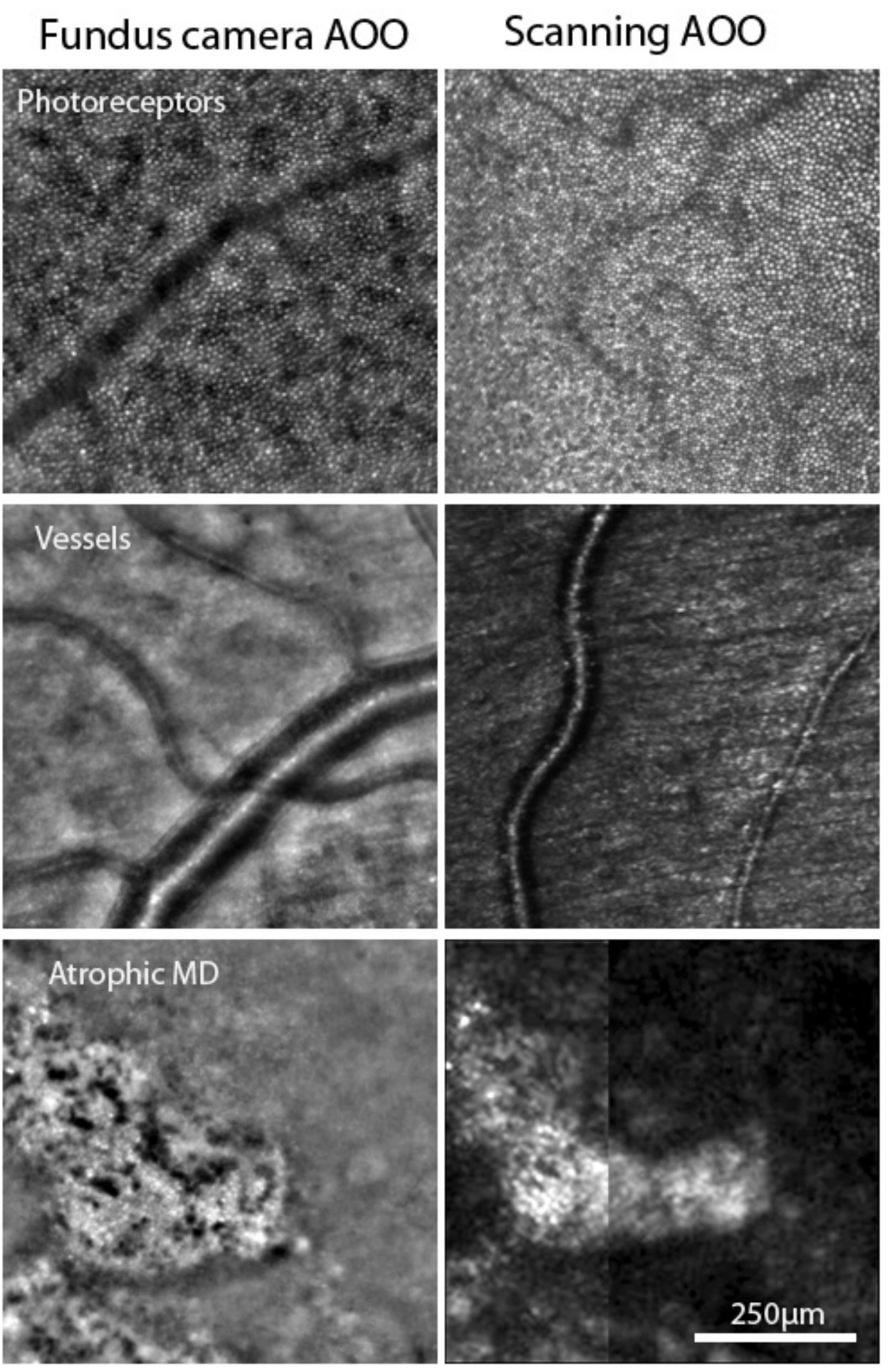
Fundus camera AOO
Scanning AOO
Photoreceptors
Vessels
Atrophic MD
250µm

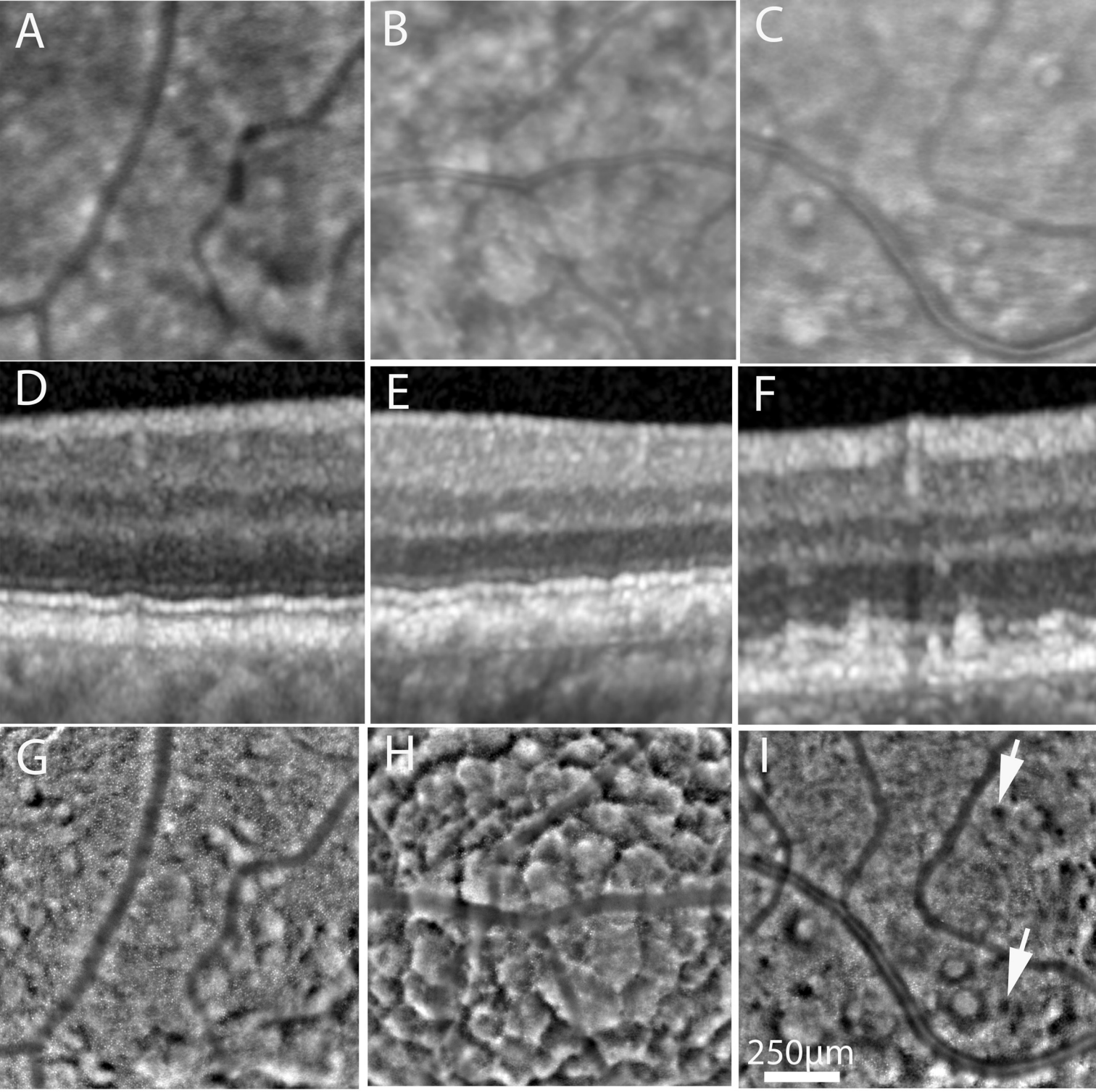
A
B
C
D
E
F
G
H
I
250µm

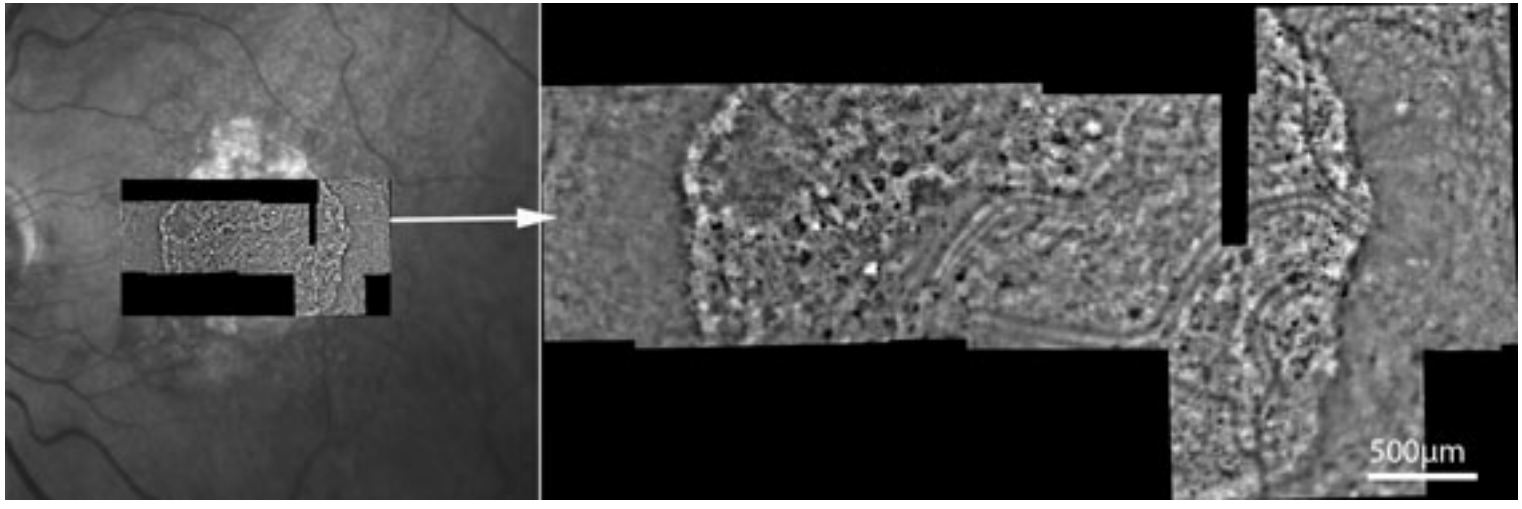
500µm

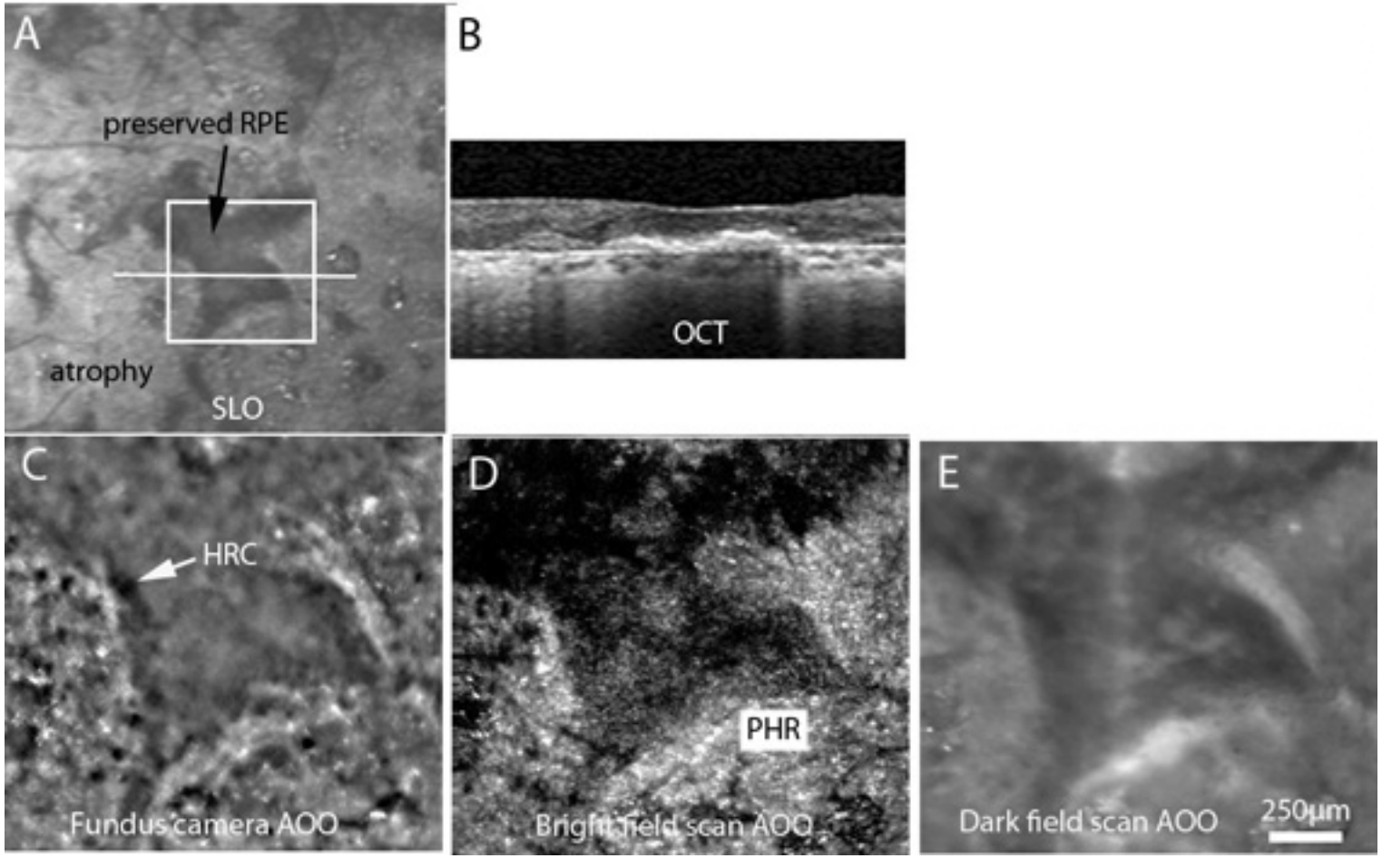
A
preserved RPE
atrophy
SLO
B
OCT
C
HRC
Fundus camera AOO
D
PHR
Bright field scan AOO
E
Dark field scan AOO
250µm

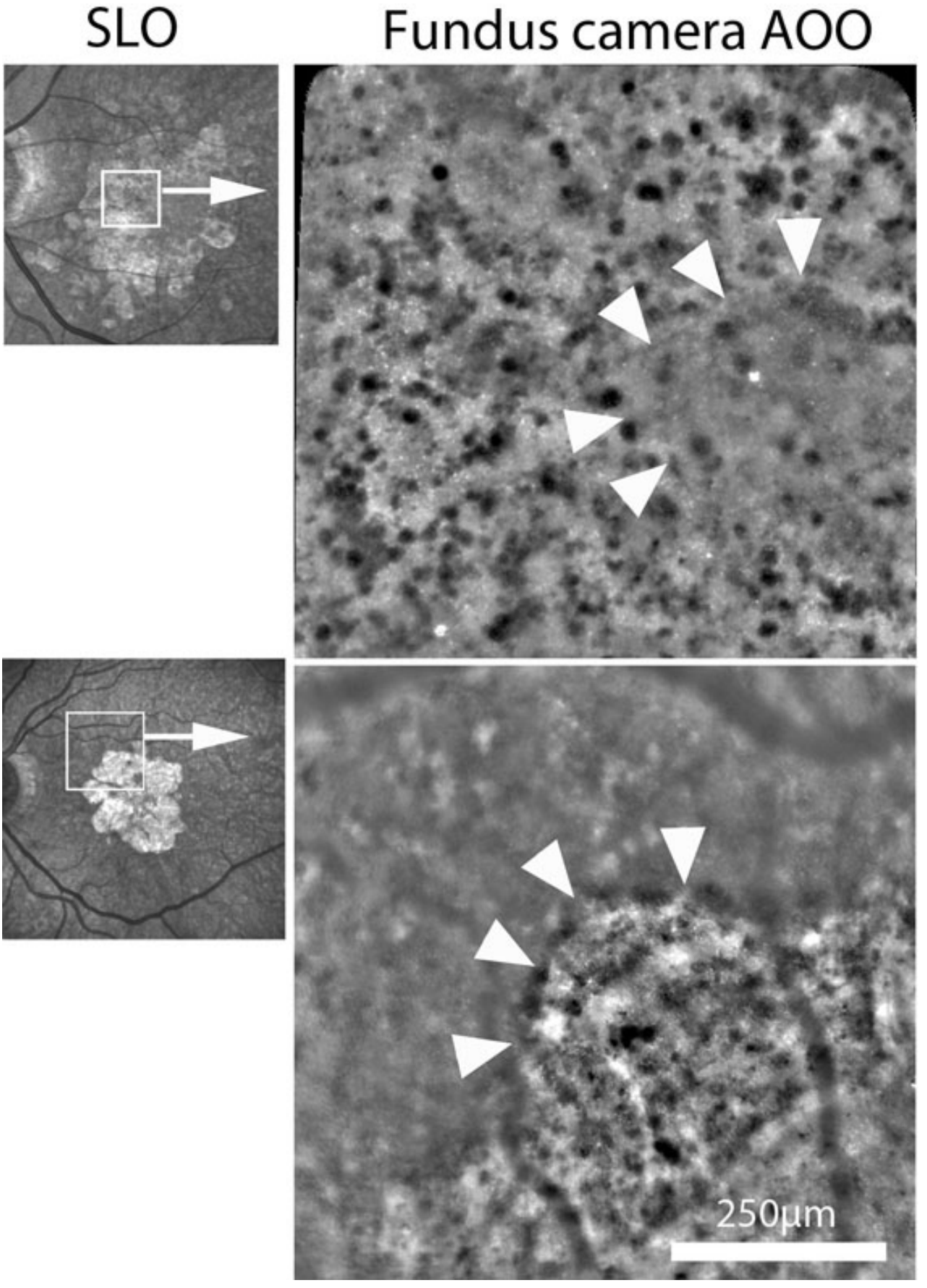
SLO
Fundus camera AOO
250µm

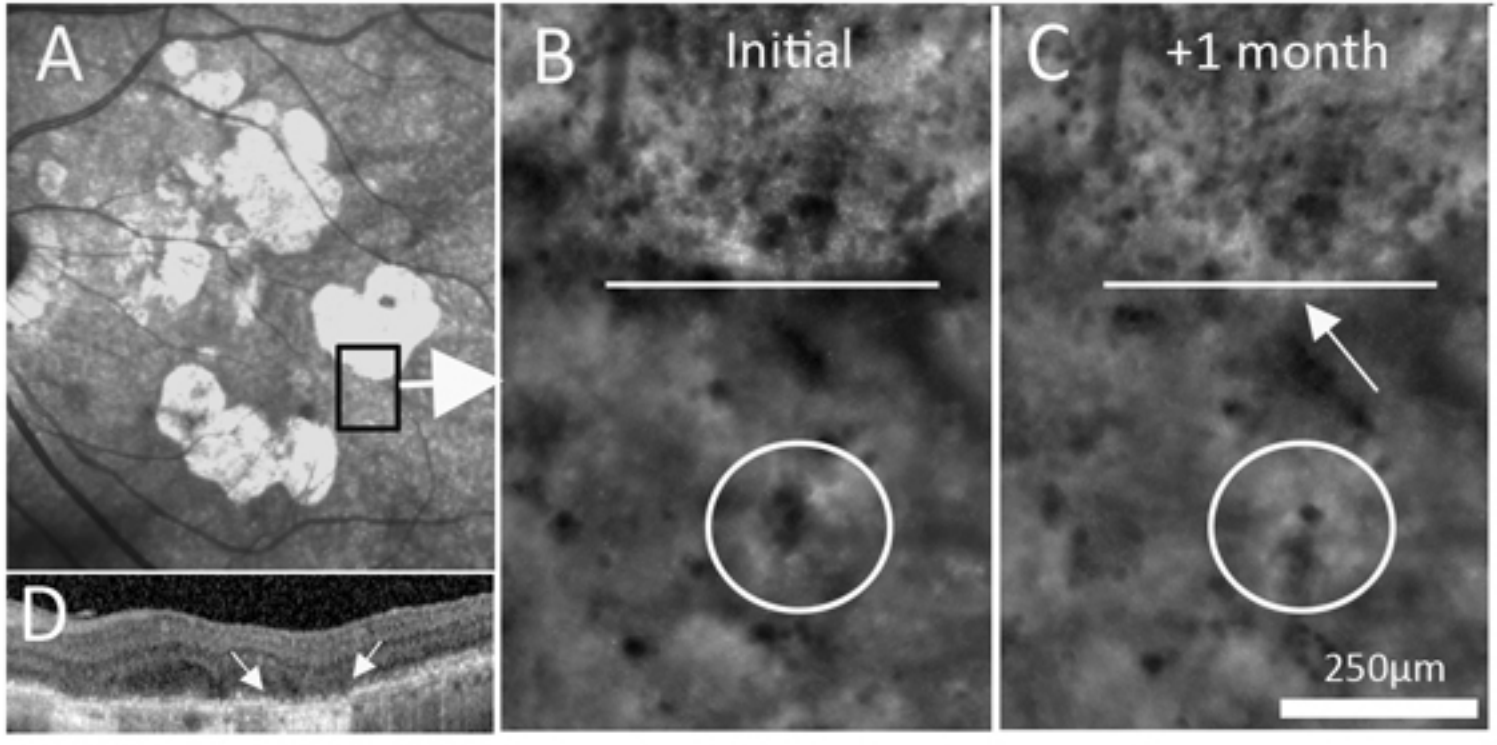
A
B
Initial
C
+1 month
D
250μm

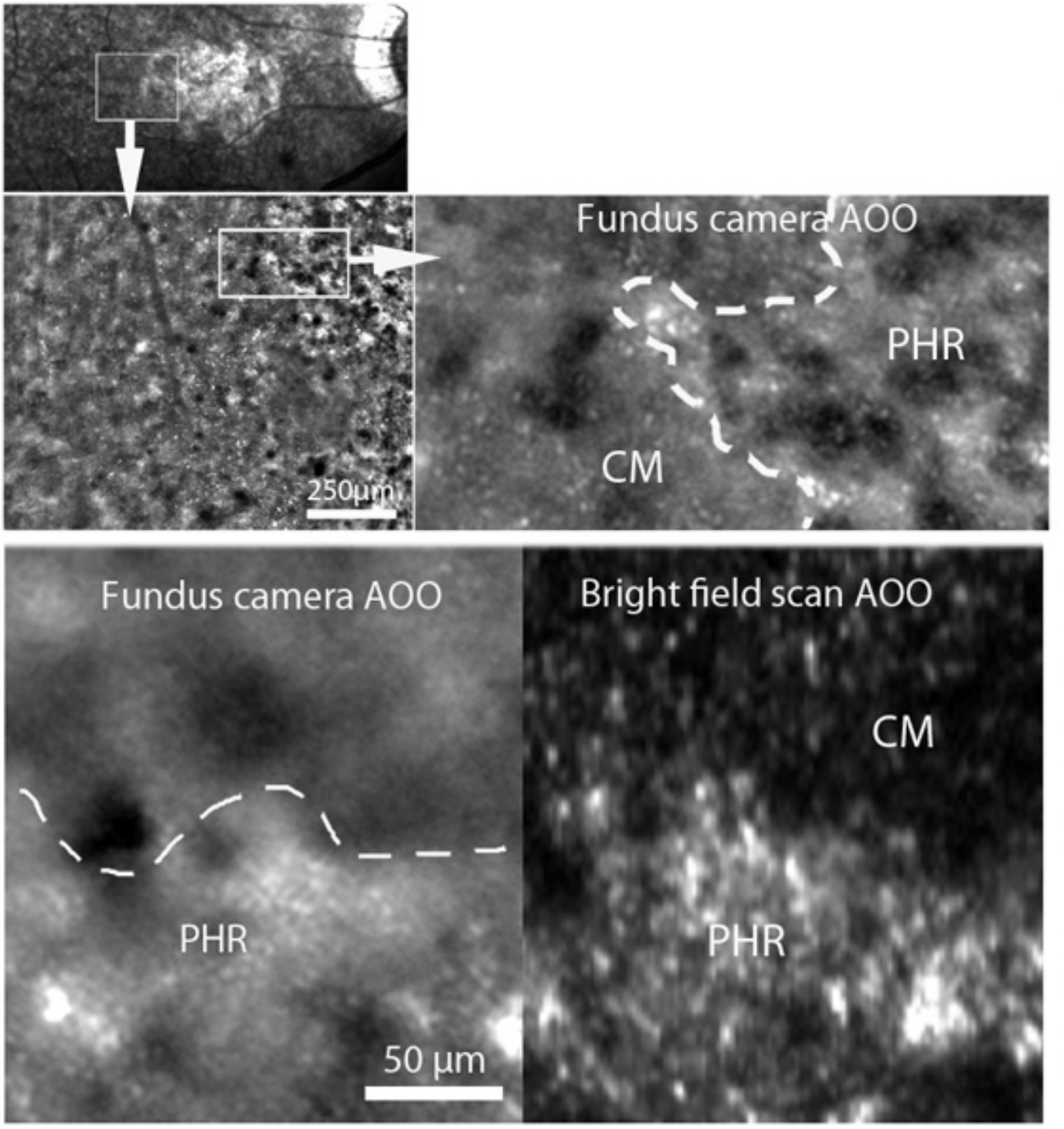
Fundus camera AOO
PHR
CM
250µm
Fundus camera AOO
PHR
50 µm
Bright field scan AOO
CM
PHR

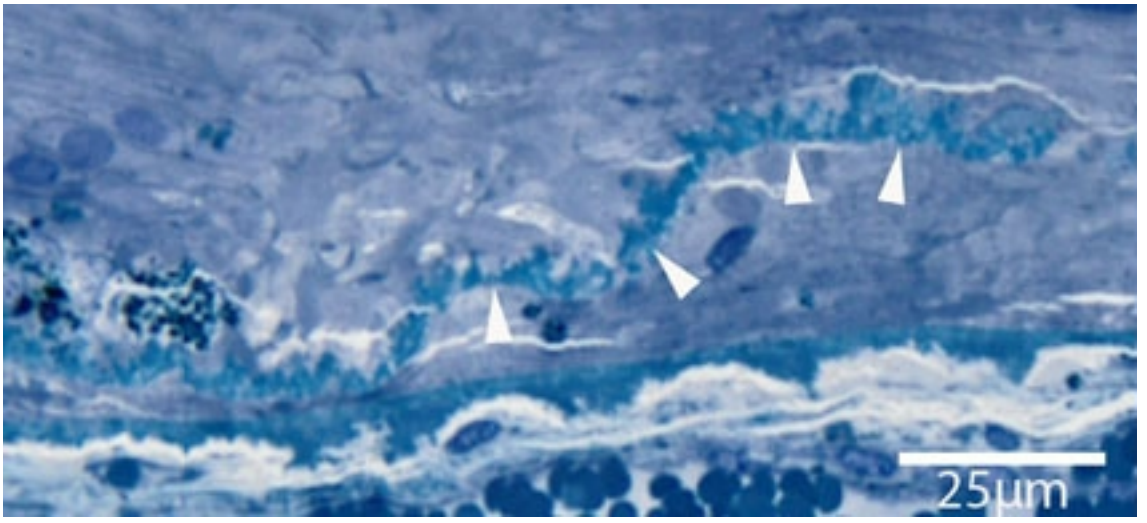
25µm

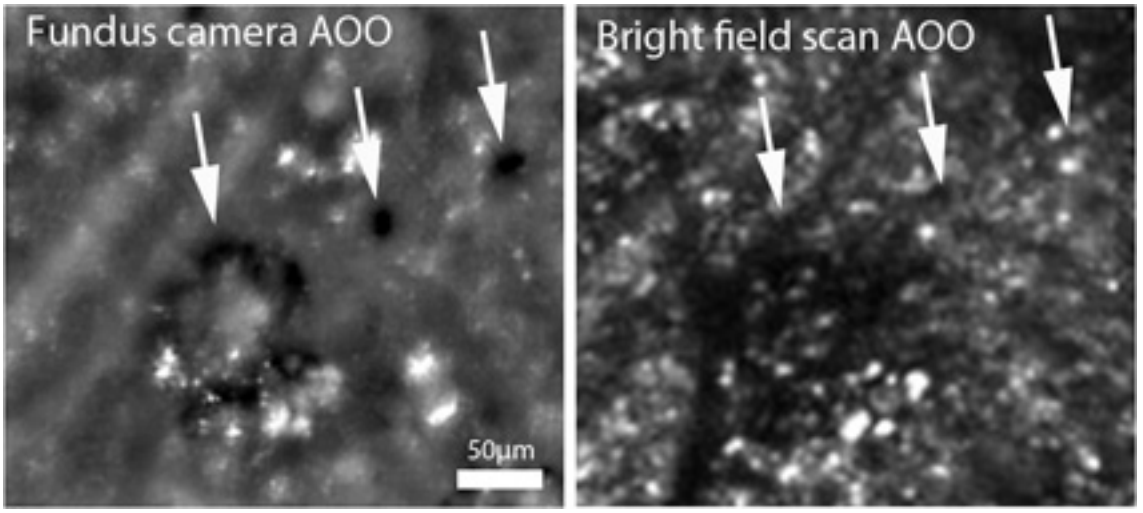
Fundus camera AOO
50µm
Bright field scan AOO

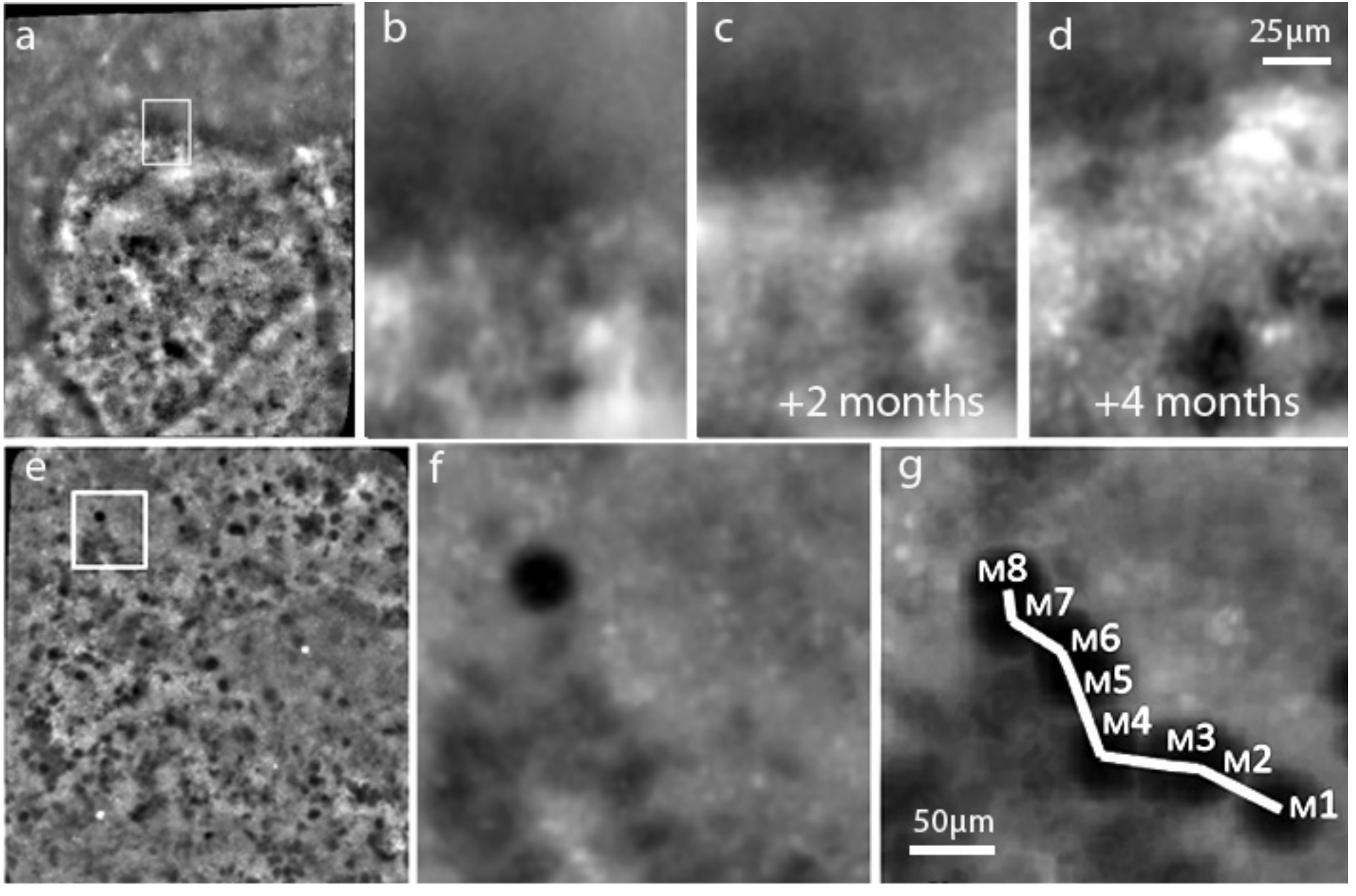
a
b
c
+2 months
d
25µm
+4 months
e
f
g
M8
M7
M6
M5
M4
M3
M2
M1
50µm

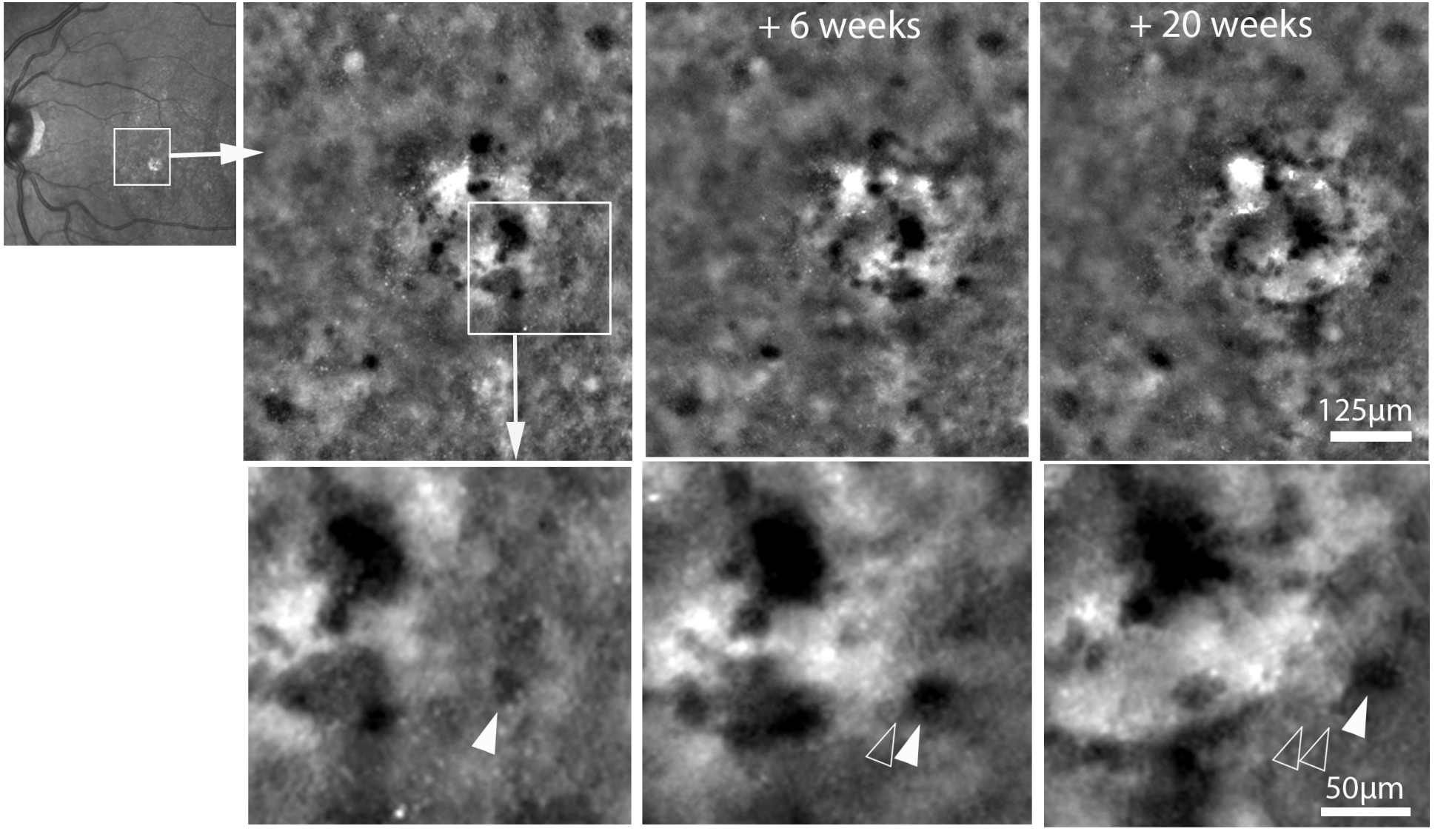
+ 6 weeks
+ 20 weeks
125µm
50µm

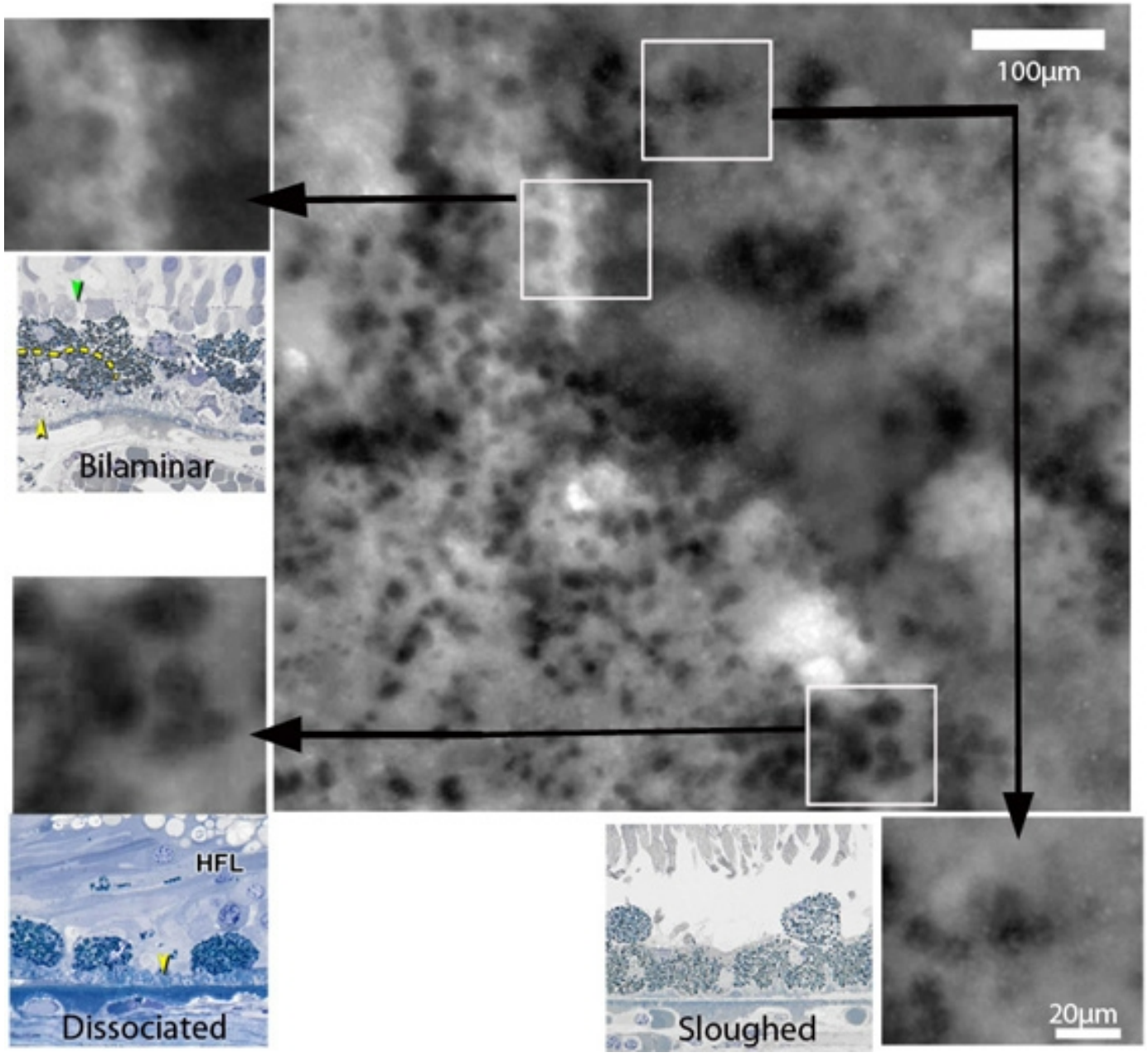
100µm
Bilaminar
HFL
Dissociated
Sloughed
20µm

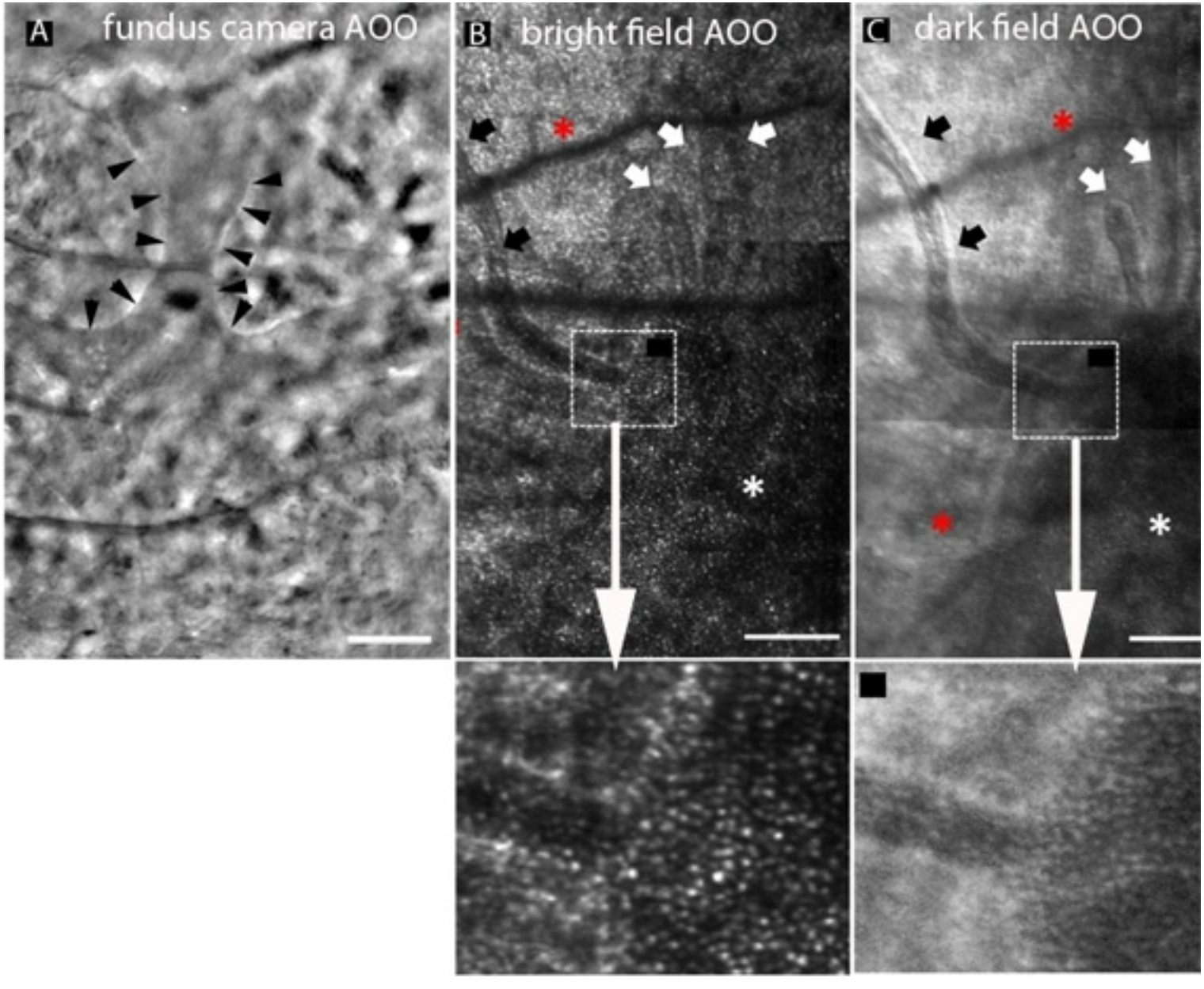
A
fundus camera AOO
B
bright field AOO
C
dark field AOO

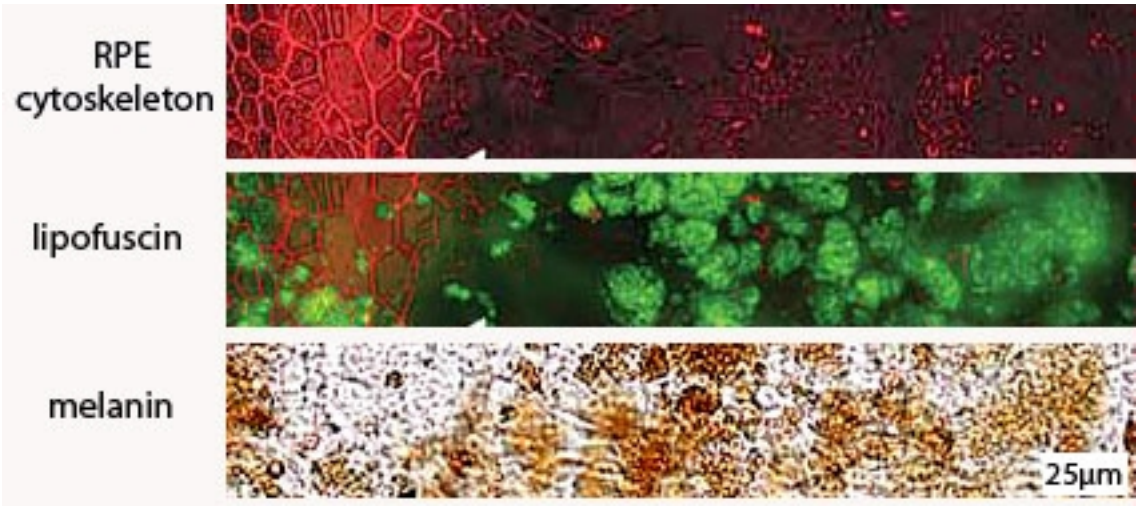
RPE
cytoskeleton
lipofuscin
melanin
25µm

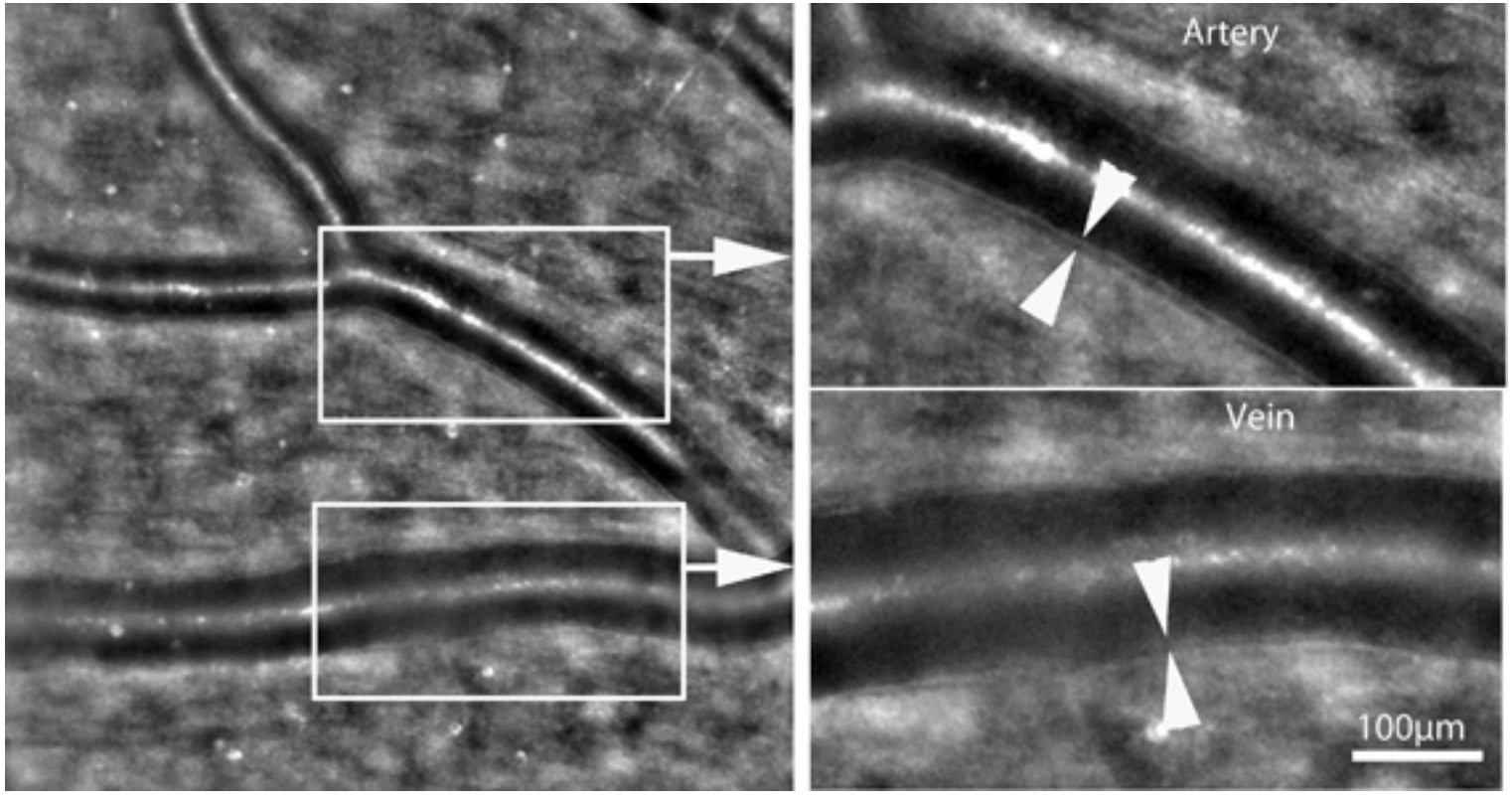
Artery
Vein
100µm

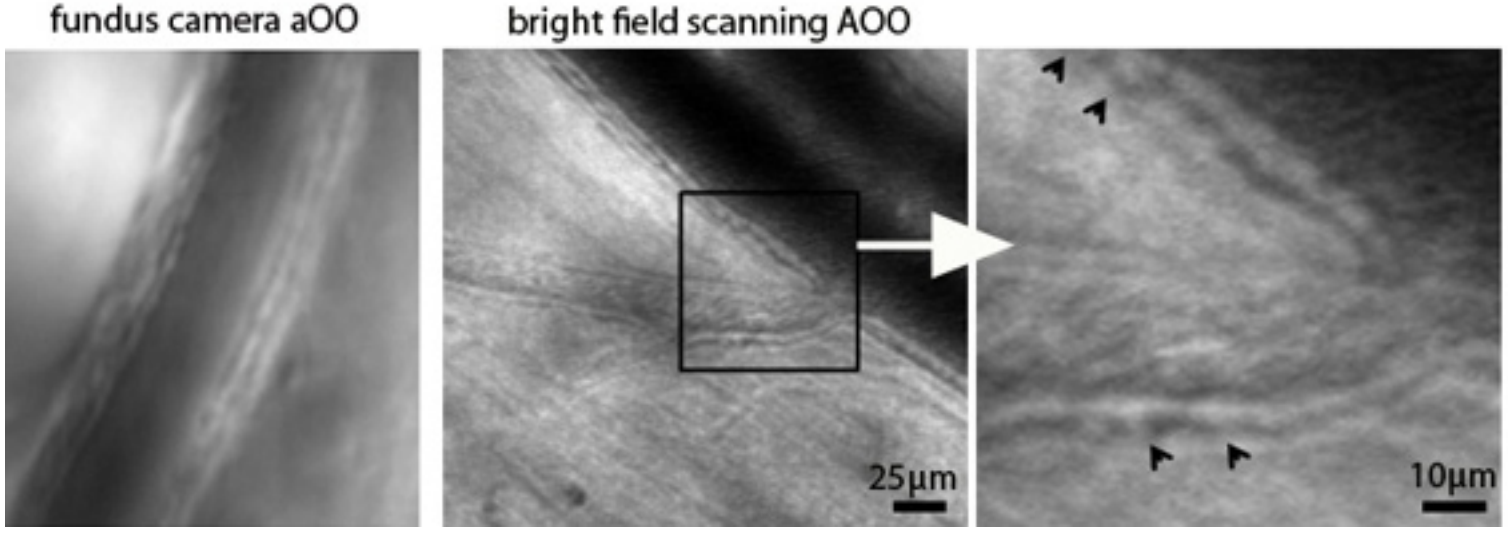
fundus camera aOO
bright field scanning AOO
25µm
10µm

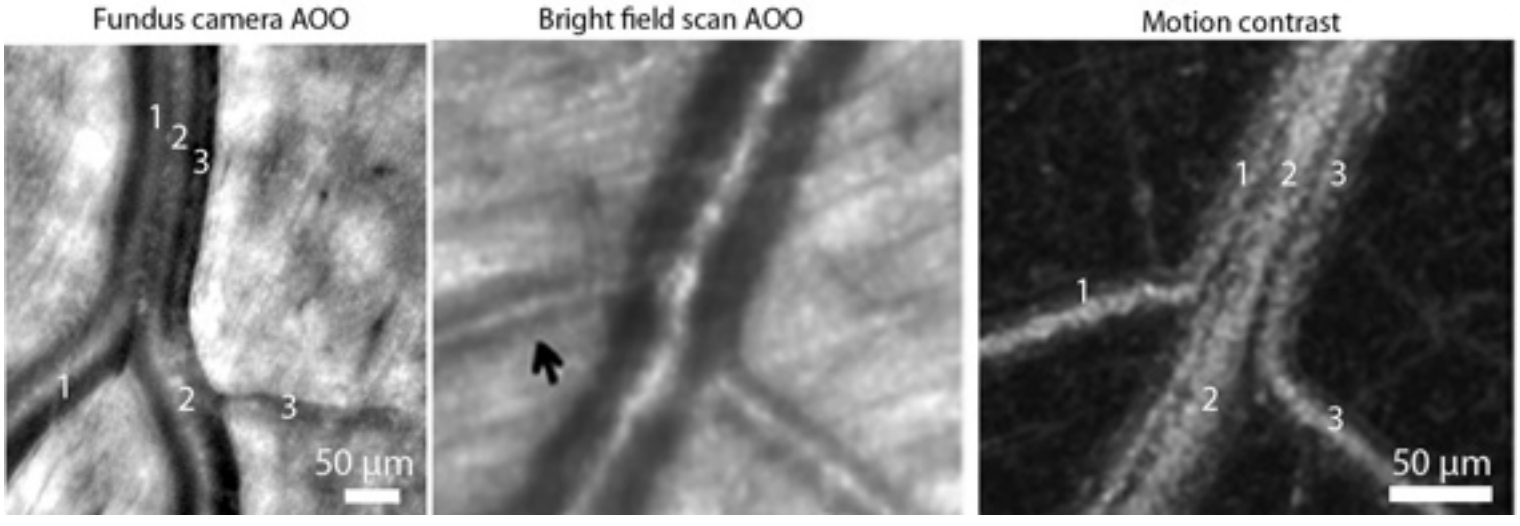
Fundus camera AOO
Bright field scan AOO
Motion contrast
1
2
3
1
2
3
50 µm
1
2
3
1
2
3
50 µm

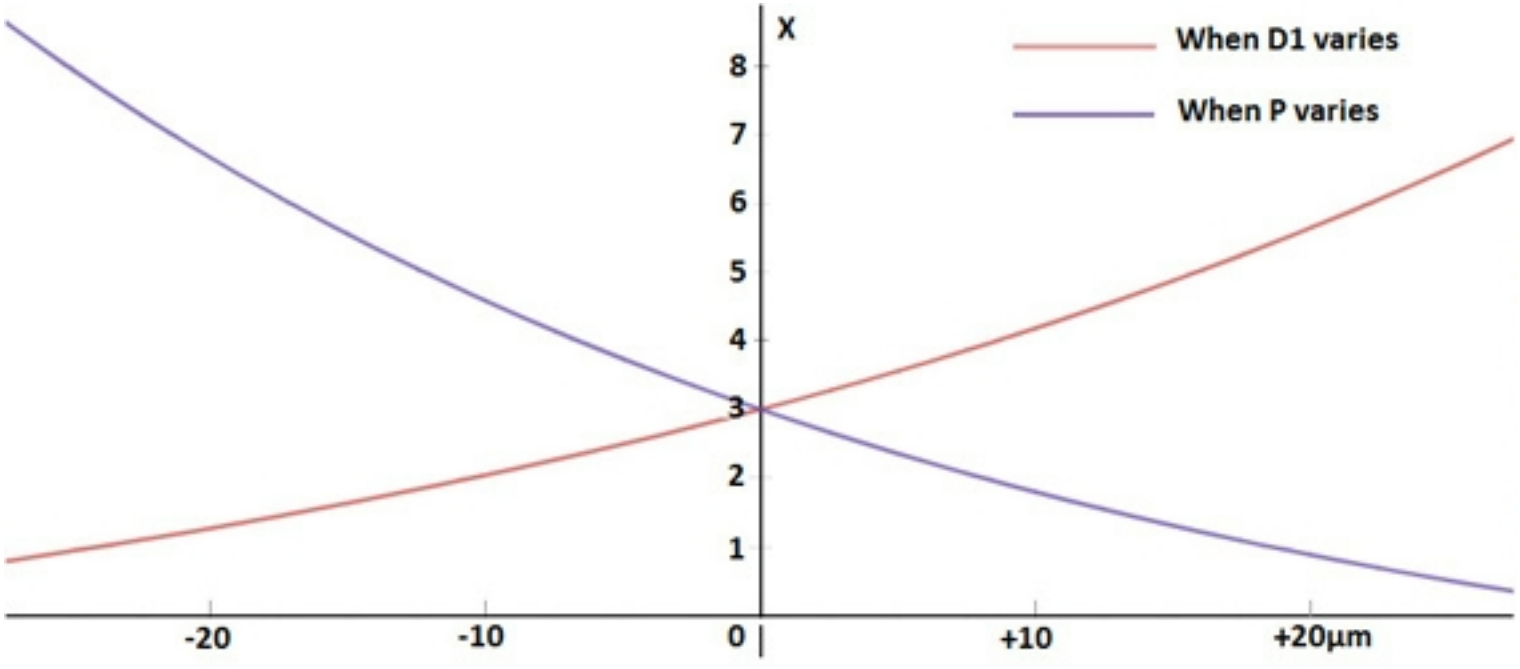
X
When D1 varies
When P varies
8
7
6
5
4
3
2
1
-20
-10
0
+10
+20µm

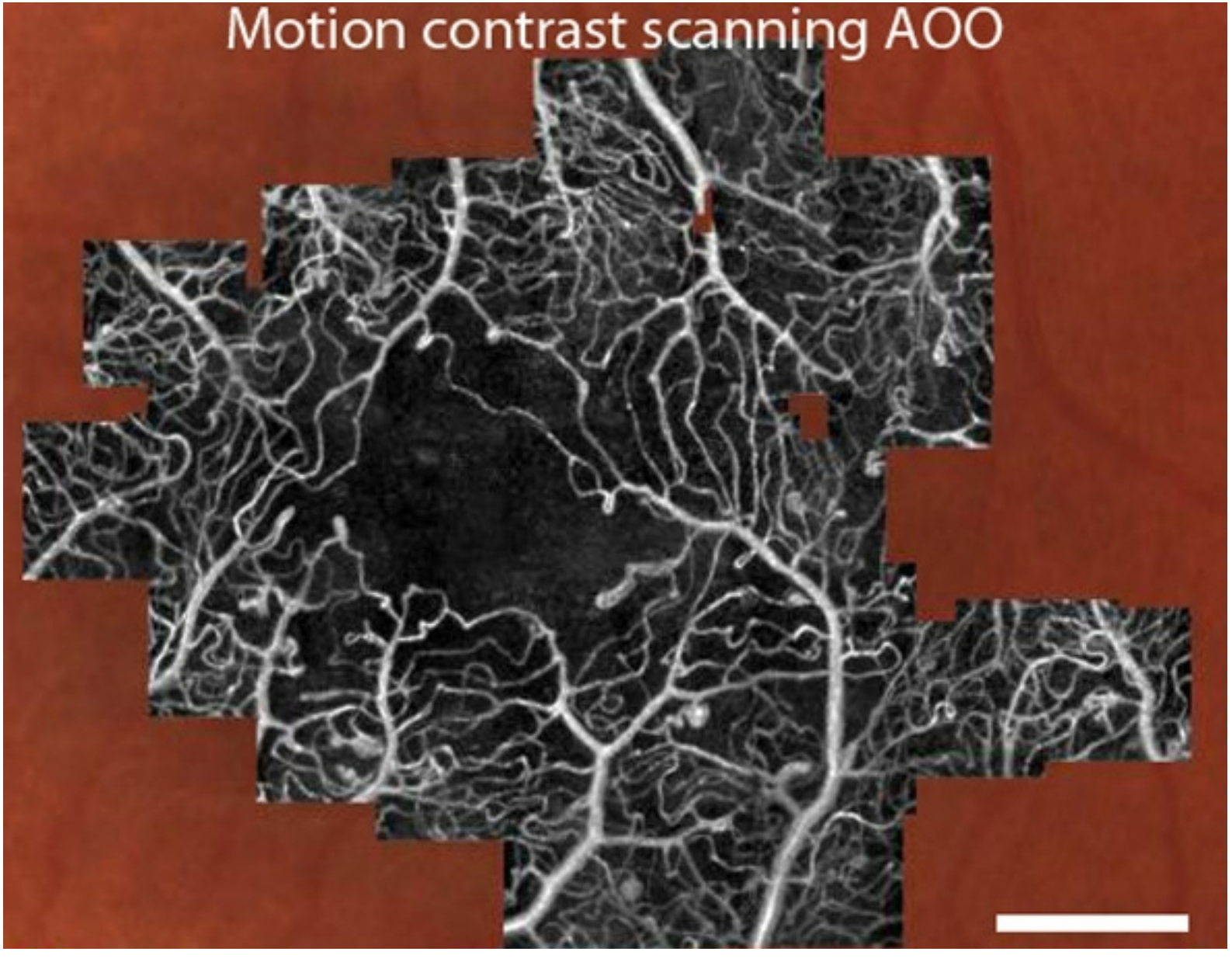
Motion contrast scanning AOO

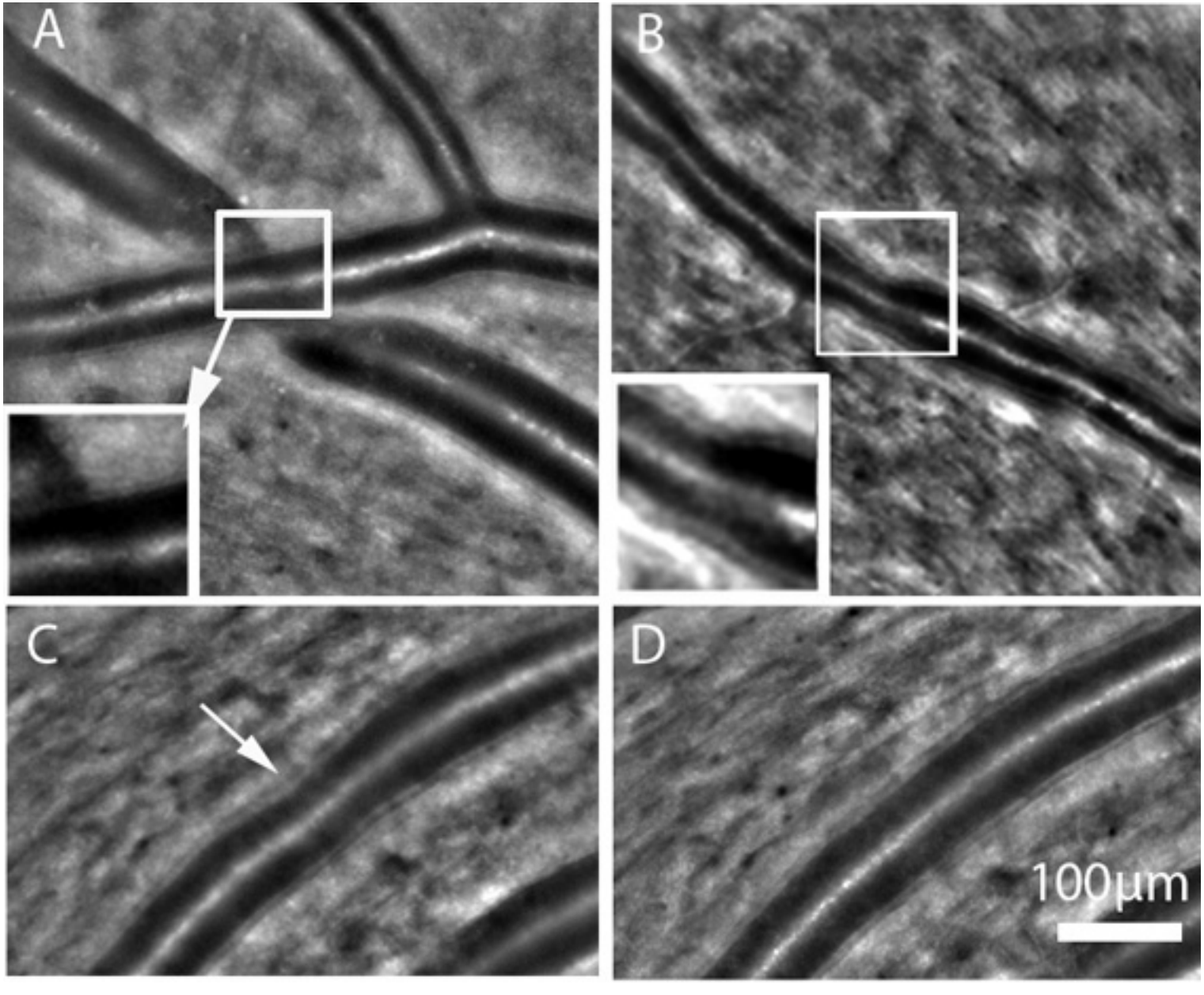
A
B
C
D
100µm

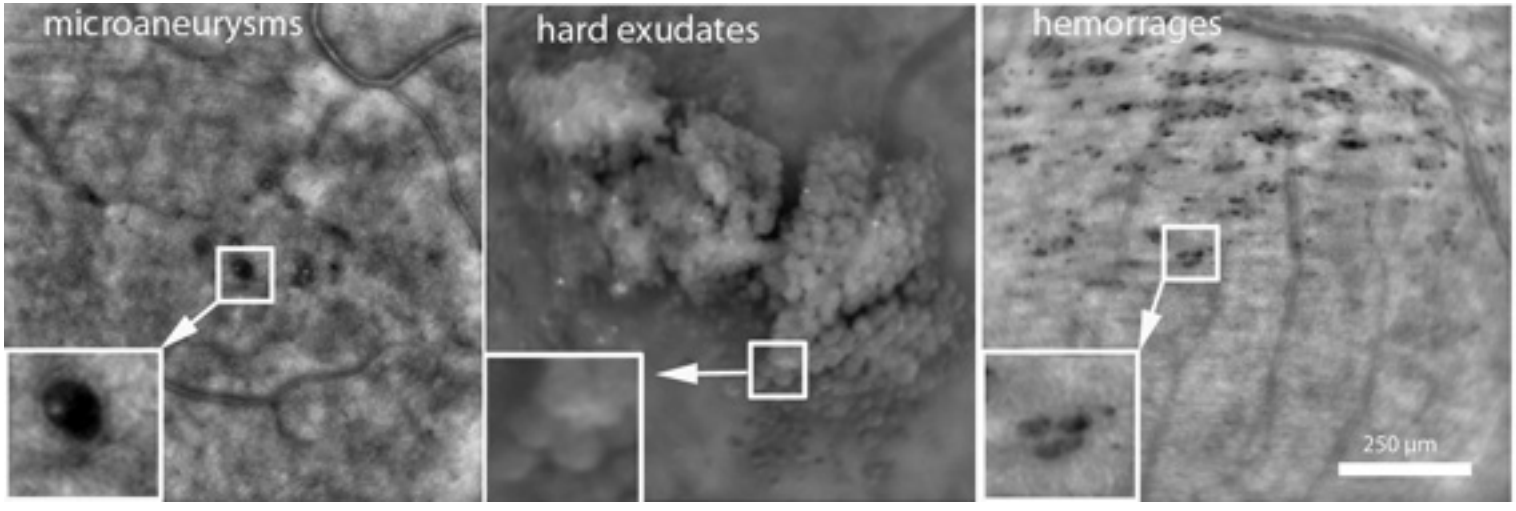
microaneurysms
hard exudates
hemorrages
250 µm

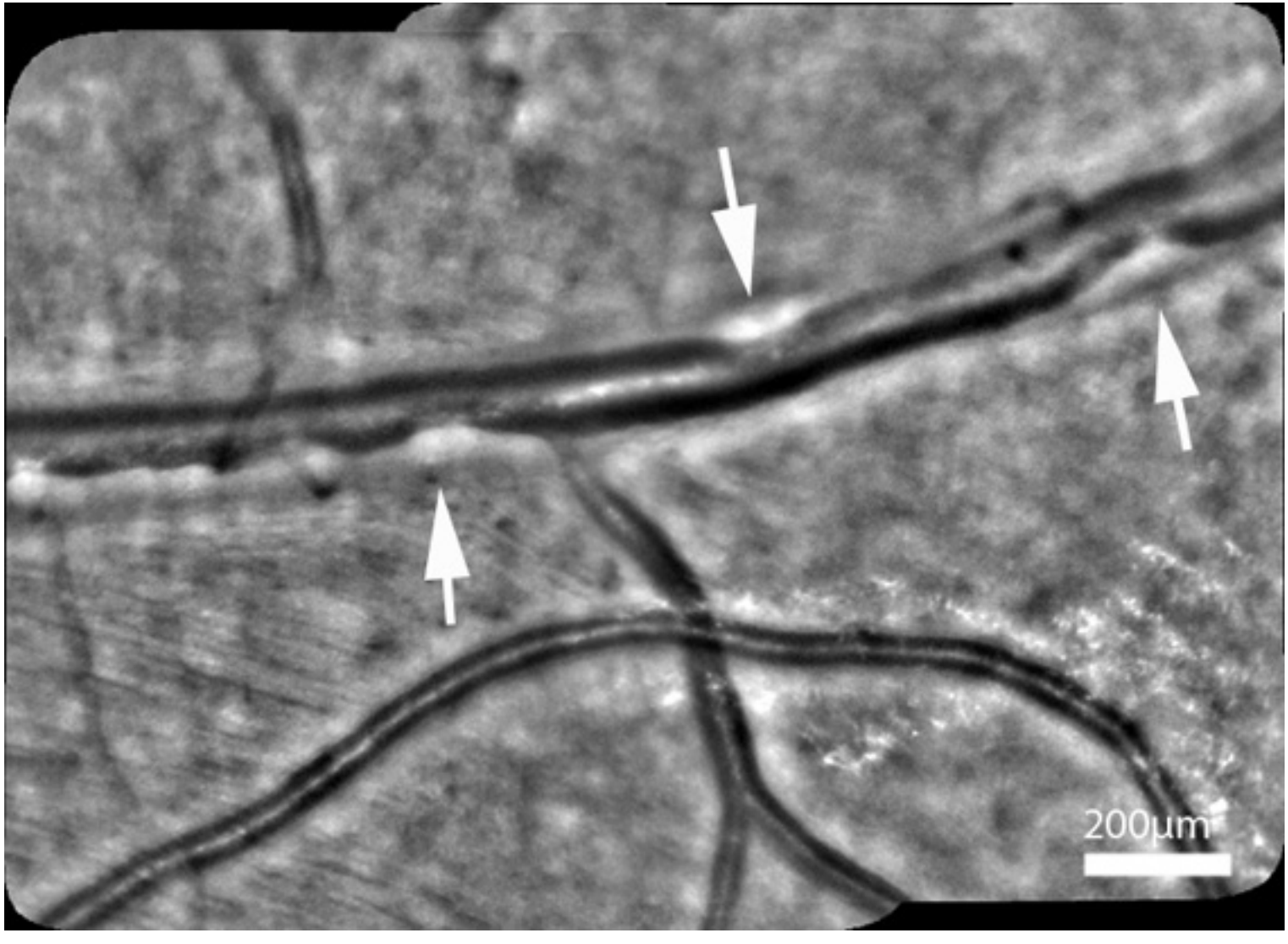
200µm

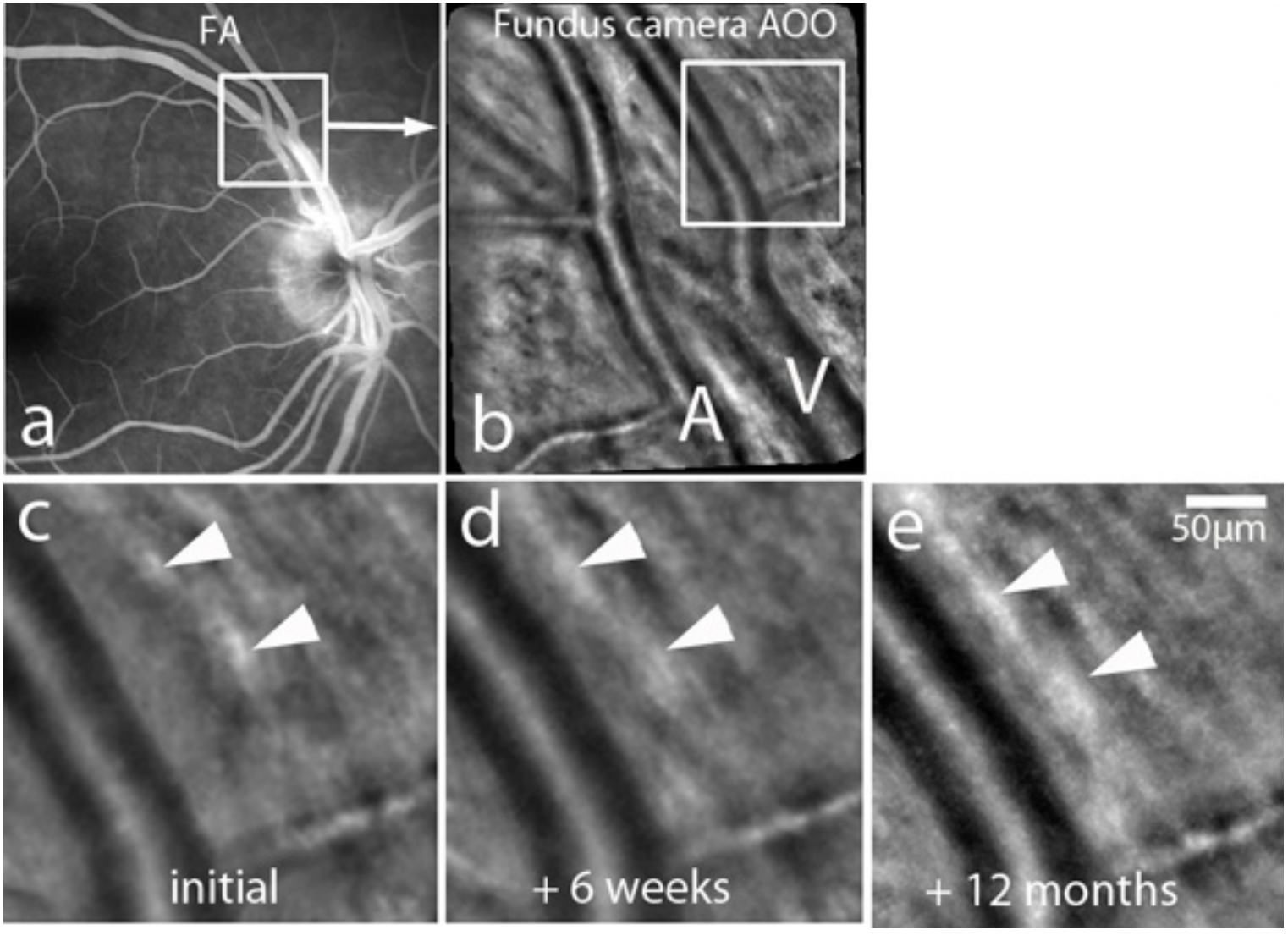
FA
a
Fundus camera AOO
b
A
V
c
initial
d
+ 6 weeks
e
50µm
+ 12 months